AD-A140 428 BOUNDARY CONDITION AND STRAIN-RATE EFFECTS ON THE RESPONSE OF BLAST-LOADE..(U) ARMY ARMAMENT RESEARCH AND DEVELOPMENT CENTER ABERDEEN PROVIN.. 1/1

UNCLASSIFIED N J HUFFINGTON ET AL. MAR 84 ARBRL-TR-02551 F/G 19/4 NL

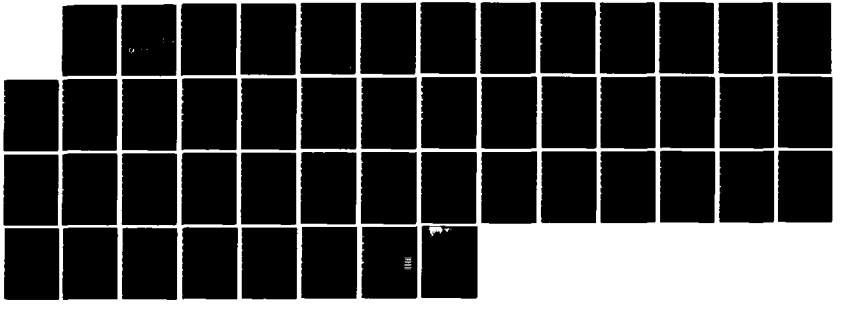

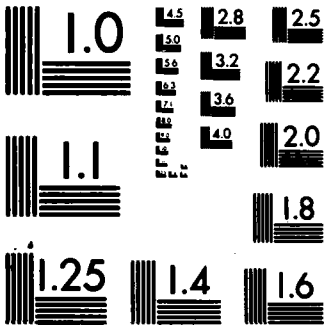

(12)

AD

AD A140428

TECHNICAL REPORT ARBRL-TR-02551

BOUNDARY CONDITION AND STRAIN-RATE EFFECTS ON THE RESPONSE OF BLAST-LOADED BEAMS

Norris J. Huffington, Jr.
John D. Wortman

March 1984

US ARMY ARMAMENT RESEARCH AND DEVELOPMENT CENTER
BALLISTIC RESEARCH LABORATORY
ABERDEEN PROVING GROUND, MARYLAND

Destroy this report when it is no longer needed.
Do not return it to the originator.

Additional copies of this report may be obtained from the National Technical Information Service, U. S. Department of Commerce, Springfield, Virginia 22161.

The findings in this report are not to be construed as an official Department of the Army position, unless so designated by other authorized documents.

The use of trade names or manufacturers' names in this report does not constitute indorsement of any commercial product.

UNCLASSIFIED

SECURITY CLASSIFICATION OF THIS PAGE *(When Data Entered)*

REPORT DOCUMENTATION PAGE		READ INSTRUCTIONS BEFORE COMPLETING FORM
1. REPORT NUMBER Technical Report ARBRL-TR- 02551	2. GOVT ACCESSION NO. ADA140428	3. RECIPIENT'S CATALOG NUMBER
4. TITLE *(and Subtitle)* BOUNDARY CONDITION AND STRAIN-RATE EFFECTS ON THE RESPONSE OF BLAST-LOADED BEAMS		5. TYPE OF REPORT & PERIOD COVERED FINAL 6. PERFORMING ORG. REPORT NUMBER
7. AUTHOR(s) Norris J. Huffington, Jr. John D. Wortman		8. CONTRACT OR GRANT NUMBER(s)
9. PERFORMING ORGANIZATION NAME AND ADDRESS US Army Ballistic Research Laboratory, ARDC ATTN: DRSMC-BLT(A) Aberdeen Proving Ground, MD 21005		10. PROGRAM ELEMENT, PROJECT, TASK AREA & WORK UNIT NUMBERS 1L161102AH43
11. CONTROLLING OFFICE NAME AND ADDRESS US Army AMCCOM, ARDC Ballistic Research Laboratory, ATTN: DRSMC-BLA-S(A) Aberdeen Proving Ground, MD 21005		12. REPORT DATE March 1984 13. NUMBER OF PAGES 47
14. MONITORING AGENCY NAME & ADDRESS*(if different from Controlling Office)*		15. SECURITY CLASS. *(of this report)* UNCLASSIFIED 15a. DECLASSIFICATION/DOWNGRADING SCHEDULE

16. DISTRIBUTION STATEMENT *(of this Report)*

Approved for public release, distribution unlimited.

17. DISTRIBUTION STATEMENT *(of the abstract entered in Block 20, if different from Report)*

18. SUPPLEMENTARY NOTES

19. KEY WORDS *(Continue on reverse side if necessary and identify by block number)*

Structural Response	Coulomb Friction	Hopkinson Bar Tests
Boundary Conditions	Rotatory Inertia	Aluminum Alloy 3003
Strain-Rate Effects	Air Blast Loading	Shear Reactions
Material Constitutive Equations	REPSIL Code	Beam Deformations

20. ABSTRACT *(Continue on reverse side if necessary and identify by block number)*

New interpretations to the results from previously reported air blast-loaded beam tests are derived, based on computations using a modified finite difference large amplitude elastoplastic beam response code which now includes a new strain-rate dependent constitutive model plus associated dynamic material data and revisions to better simulate the physical support conditions, including frictional and rotatory inertia effects.

DD FORM 1 JAN 73 1473 EDITION OF 1 NOV 65 IS OBSOLETE

UNCLASSIFIED

SECURITY CLASSIFICATION OF THIS PAGE *(When Data Entered)*

TABLE OF CONTENTS

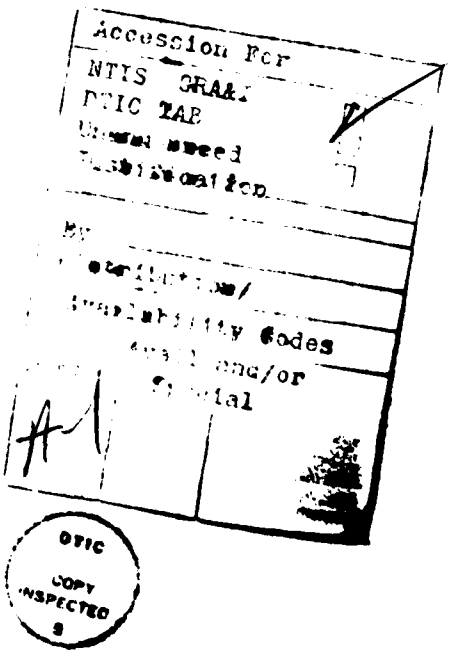

LIST OF ILLUSTRATIONS

LIST OF TABLES

I. INTRODUCTION

Under sponsorship by the US Navy Civil Engineering Laboratory (CEL) the Ballistic Research Laboratory (BRL) conducted an experimental investigation of the structural response of metallic beams of rectangular cross-section to air blast loading.[1] The specimens and a support fixture intended to provide simply supported end conditions were supplied by CEL. Pre-test predictions of beam responses were performed at BRL, principally for use in the design of instrumentation. These predictions employed static material property data and empirical air blast parameters in conjunction with the REPSIL structural response computer program.[2] When the experimental data became available it was found that the pre-test calculations overpredicted the response by as much as a factor of four. This was cause for some chagrin since the response methodology had been previously validated by comparisons with experimental results in numerous applications. In the conclusions to the Technical Report[1] on this investigation it was speculated that the discrepancies were due to

(a) significant strain-rate effects in the specimen material and/or

(b) neglect of frictional and rotatory inertia effects at the support points which resulted in resisting moments at the beam boundaries.

Subsequent to publication of Reference 1, dynamic material constitutive data were obtained for the beam material. These data were the results of a series of split Hopkinson bar tests on both tension and compression specimens. An interpretation and an analytical modeling of these data are presented in Chapter II. Following this a detailed formulation which includes the effects of rotatory inertia of the rocker shafts and friction at bearing interfaces is given in Chapter III. Then, in Chapter IV, this augmented boundary condition formulation and the dynamic material constitutive modeling are employed within the REPSIL code for a reassessment of the comparison between predictions and experimental response.

II. DYNAMIC MATERIAL PROPERTIES

The beam specimens furnished by CEL were only identified as being fabricated from 3003 aluminum alloy. When the cited discrepancies between experimental responses and predictions became evident, specimens for both tensile and compressive split Hopkinson bar tests were machined at BRL from unused specimens. These dynamic test specimens were forwarded to the University of

---

[1] *C. N. Kingery, N. J. Huffington, Jr., and J. D. Wortman, "Response of Beams to Airblast Loading," Ballistic Research Laboratory Technical Report ARBRL-TR-02369, September 1981. (AD B060635L)*

[2] *J. D. Wortman, "RPSL1D (A One-Dimensional Version of REPSIL)," Ballistic Research Laboratory Memorandum Report ARBRL-MR-03221, November 1982. (AD A122336)*

Dayton Research Institute (UDRI) through the Air Force Materials Laboratory for use in their facility. A digest of the material test data produced by UDRI[3,4] follows.

Figure 1(a) shows representative uniaxial transient values of engineering stress σ, engineering strain ε, and engineering strain rate $\dot{\varepsilon}$ for a tensile Hopkinson bar test. The stress-strain curve in Figure 1(b) was obtained by eliminating the time variable between the σ and ε plots in Figure 1(a). If one discounts the "noise" induced by the UDRI data reduction system it may be inferred that during most of the test there is a nearly constant value of strain rate $\dot{\varepsilon}$ and that, at least for this test, the material behavior can be characterized as elastic, perfectly plastic.

Corresponding results for a representative dynamic compression test are shown in Figure 2. For this test it may be seen that the strain rate decreases during the deformation process, although the departure from an average value is not excessive. The stress-strain behavior is approximately elastic, linear strain hardening.

Another type of result is illustrated in Figure 3. This dynamic tensile test was performed at a significantly higher impact velocity (and strain rate) than that for the result of Figure 1. The large oscillations in the stress* versus time curve are associated with wave reflections within the specimen and with non-uniform stress distribution associated with "necking." Consequently the stress-strain curve of Figure 3(b) does not represent the dependence of stress on strain which would apply to a specimen in a state of homogeneous uniaxial stress.

The results from nine Hopkinson bar tests have been converted to the stress-strain variables employed by the REPSIL code; i.e., Cauchy (true) stress τ versus Almansi strain E, using

$$E = \varepsilon(1 + \tfrac{1}{2}\varepsilon) \tag{1}$$

$$\tau = \sigma(1 + \varepsilon) \tag{2}$$

and the values thus obtained are plotted in Figure 4. It should be noted that the slope of a curve in τ versus E space is related to a σ versus ε curve by

$$\frac{d\tau}{dE} = \frac{d\sigma}{d\varepsilon} + \frac{\sigma}{1+\varepsilon} \tag{3}$$

It should be noted that the stress σ is not measured within the specimen; rather, it is calculated from strain measurements made on the surrounding elastic pressure bars.

[3]*Private communications from S. J. Bless and A. Challita, UDRI to N. J. Huffington, Jr., BRL.*

[4]*S. J. Bless, A. Challita, and A. M. Rajendran, "Dynamic Tensile Test Results for Several Metals," Air Force Material Laboratory Report AFWAL-TR-82-4056, April 1982.*

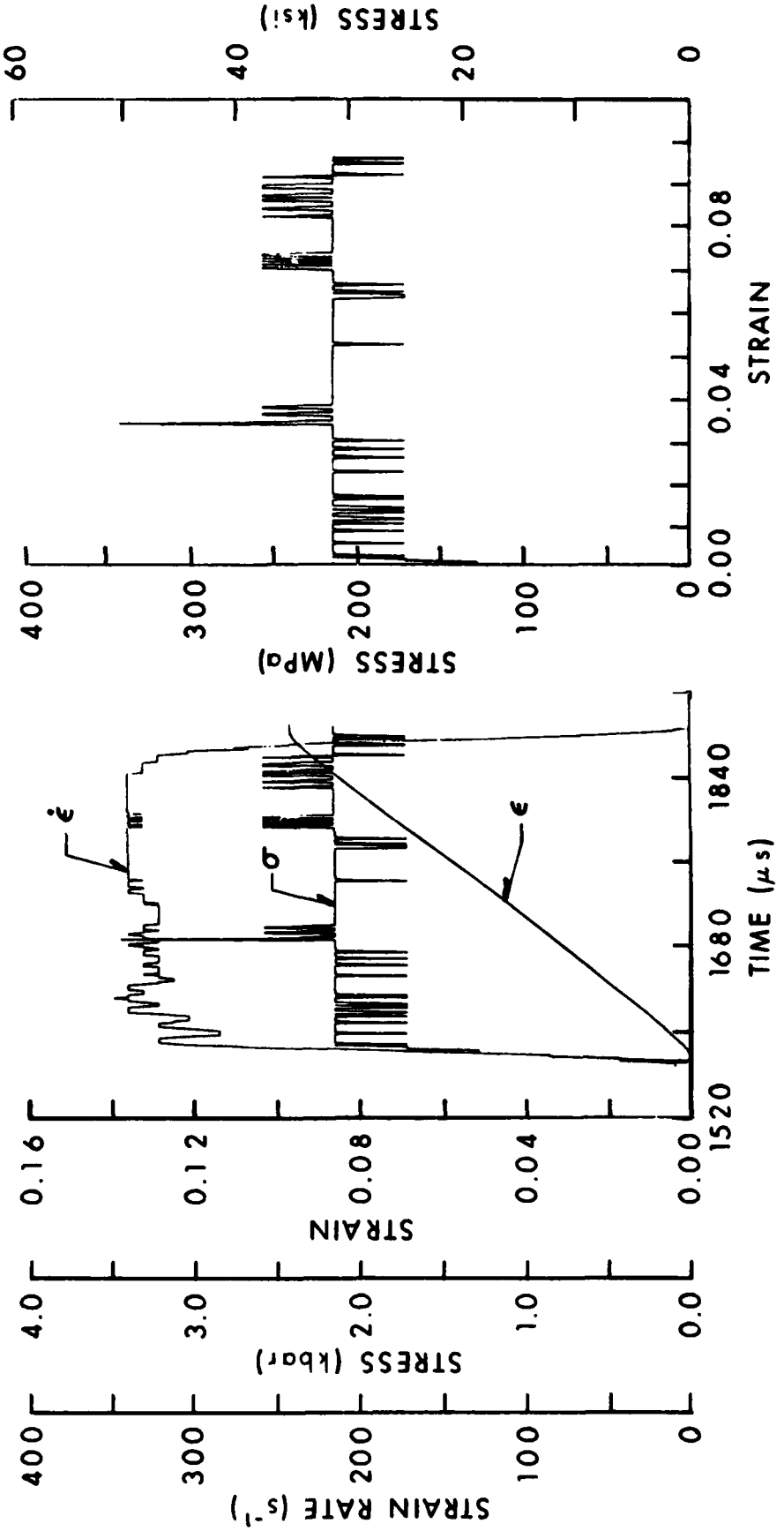

Figure 1. Results from tensile Hopkinson bar test #HB040.

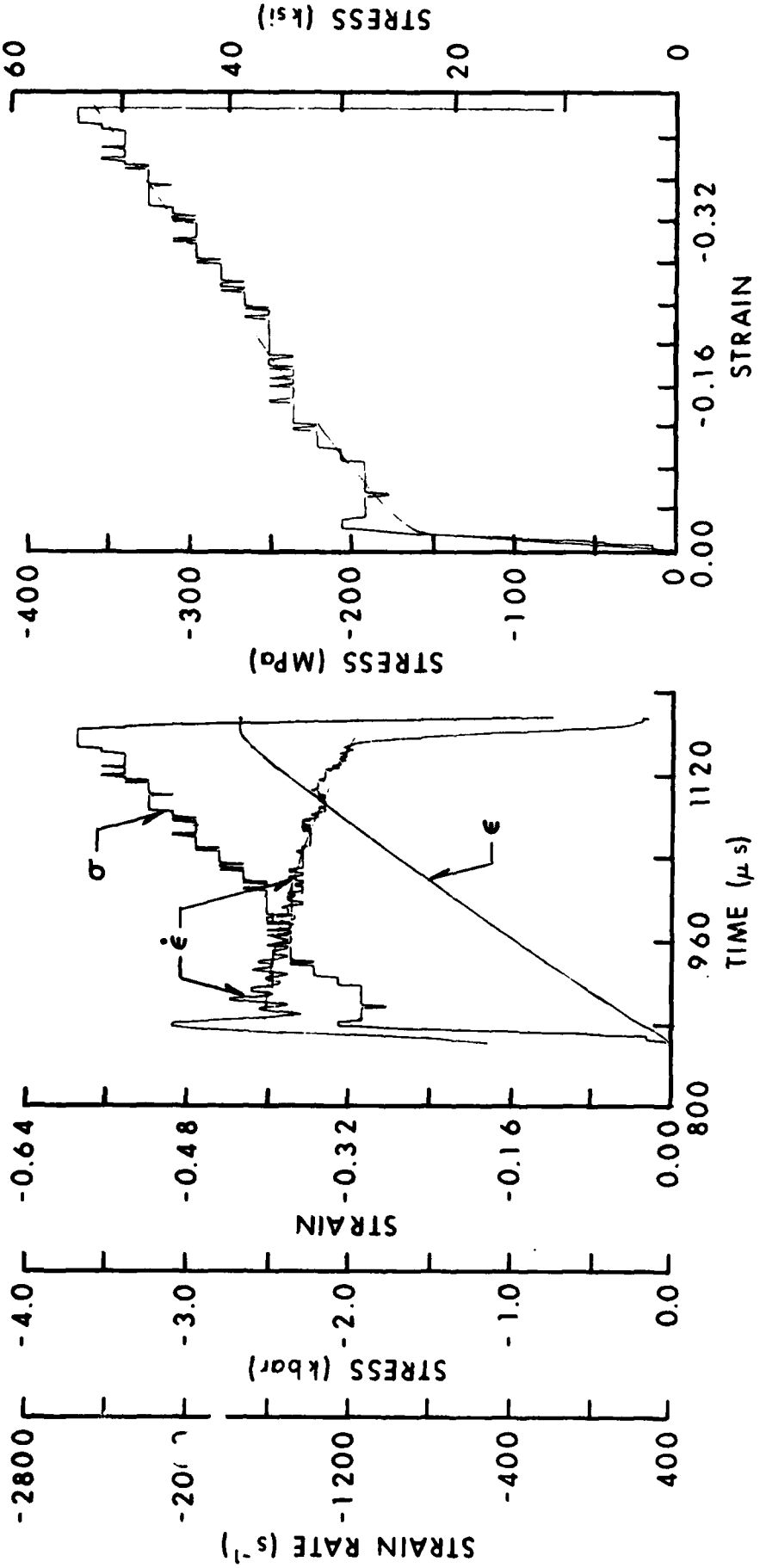

Figure 2. Results from compression Hopkinson bar test #HB057.

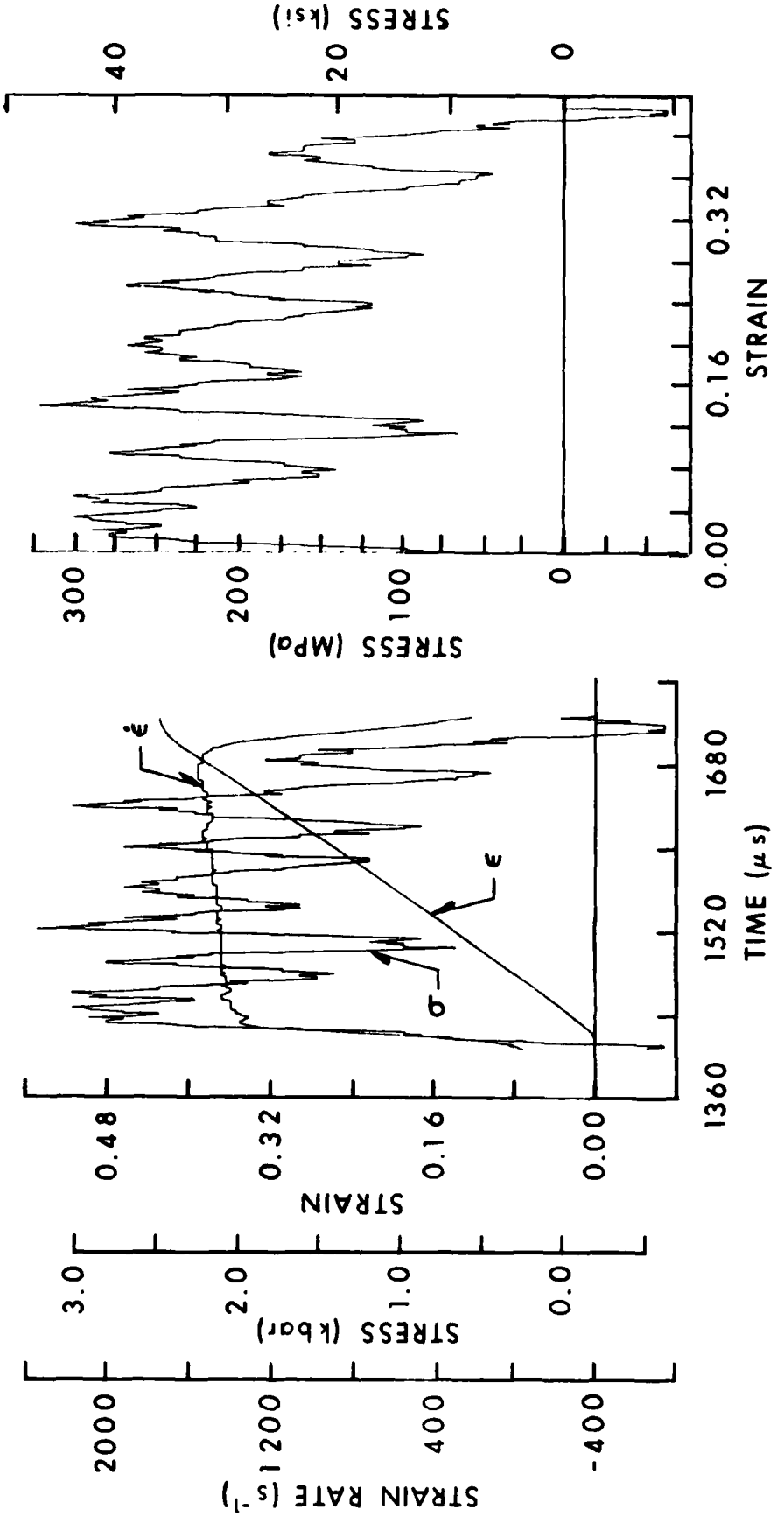

Figure 3. Results from tensile Hopkinson bar test #HB0064.

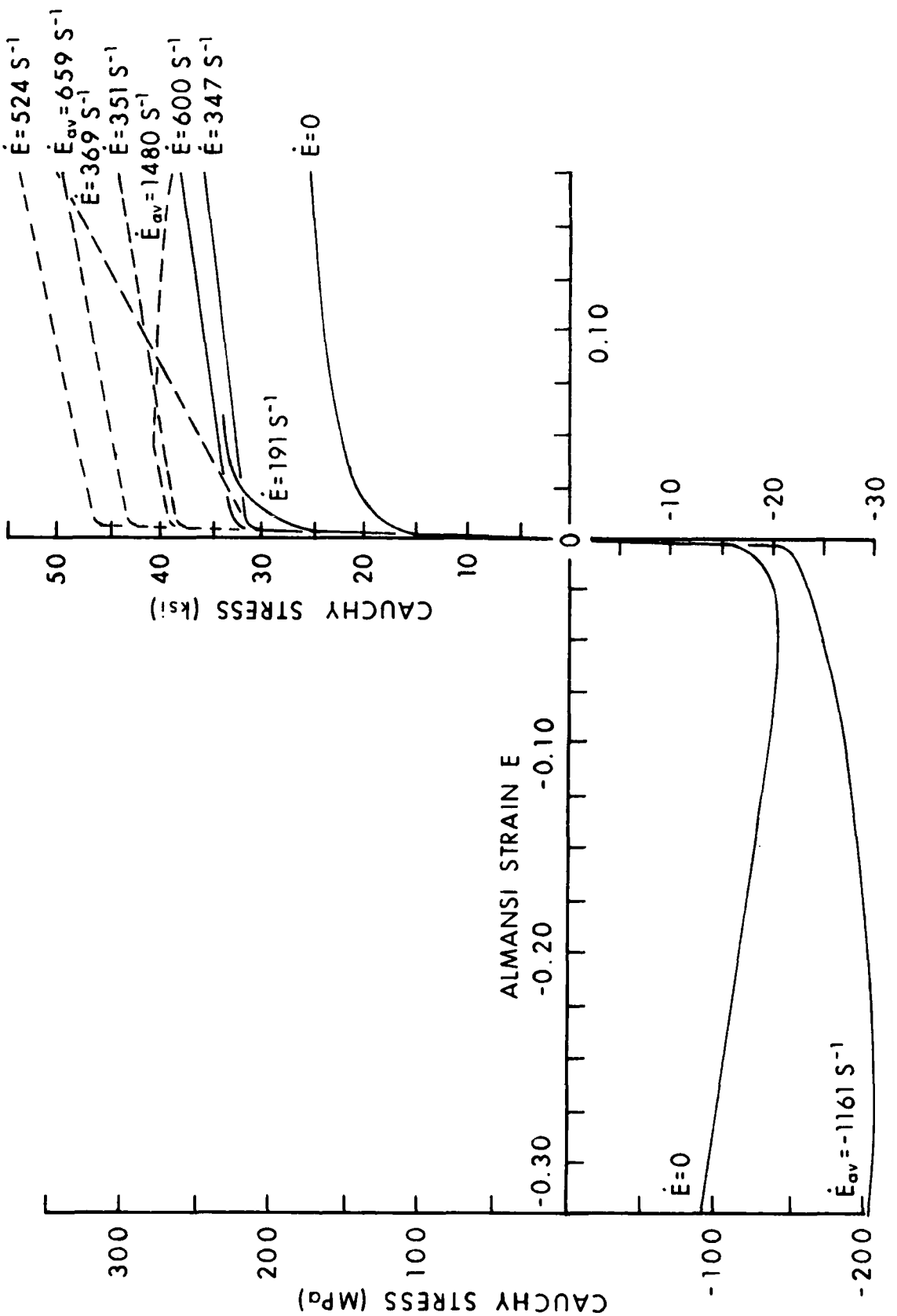

Figure 4. Stress-strain data for 3003 aluminum alloy.

Since many, but not all, of the tensile Hopkinson bar tests had the form of Figure 1(b) with $d\sigma/d\varepsilon \approx 0$ and $\varepsilon << 1$, these tensile τ versus E curves have a linear strain hardening form with slope approximately equal to the flow stress. The strain rate labels on Figure 4 are average values; in some tests the variation of $\dot{E}$ was considerable.

Obviously, there is a disconcerting amount of scatter associated with the tensile Hopkinson bar tests. It must be appreciated this test is more open to question than the compression Hopkinson bar test since it is difficult to achieve uniform stressing in a very short specimen through threaded ends. The dashed curves in Figure 4 were from tests which were regarded as less reliable or were provided belatedly. The curve labeled $\dot{E} = 1480s^{-1}$ corresponds to the data of Figure 3, where necking of the specimen occurred. The curve labeled $\dot{E} = 369s^{-1}$ was derived from a test which exhibited a significant strain hardening slope $d\sigma/d\varepsilon$. Only one compression Hopkinson curve is shown in Figure 4 since the other compression tests were conducted at a much higher impact velocity and provided no useful data in the range of E shown. These higher velocity tests did reveal a monotonic increase in the magnitude of the flow stress tending toward a saturation limit.

Figure 4 also includes a curve labeled $\dot{E} = 0$ which corresponds to the static stress-strain data published in Appendix A of Reference 1. From an examination of this figure it may be concluded that, in spite of the scatter in the dynamic tensile data, the beam specimen material is significantly rate-sensitive, entailing an increase in the dynamic flow stress of 50% to 100% over the static value.

In order for dynamic material property data to be useful in response analysis, it is necessary to incorporate these data into a mathematical rate-dependent constitutive model. In Reference 1 a single post-test response calculation was made using a power law strain-rate dependent model which was available within the REPSIL code:

$$\tau_d = \tau_s \left[1 + \left| \frac{\dot{E}}{D} \right|^{1/p} \right] \tag{4}$$

where

τ_s = static uniaxial flow stress

τ_d = dynamic uniaxial flow stress

D,p = parameters available for fitting experimental data.

At that time no dynamic data were available for the beam material so published[5] values of $D = 6500s^{-1}$ and $p = 4$ for 6061-T6 aluminum alloy were used in the

---

[5] *P. S. Symonds, "Viscoplastic Behavior in Response of Structures to Dynamic Loading," in Behavior of Materials Under Dynamic Loading, N. J. Huffington, Jr., Editor, ASME, 1965.*

response calculation. Since 6061-T6 aluminum is known to have only a slight rate-sensitivity it is not surprising that this calculated response differed by only a small amount from the response when rate effects were omitted.

The model represented by Equation (4) has a serious disadvantage for numerical calculations. Because

$$\lim_{\dot{E} \to 0} \frac{d\tau}{d\dot{E}} = \infty \text{ for } P > 1, \tag{5}$$

Equation (4) requires large jumps in the flow stress when $\dot{E}$ becomes small or changes sign. These jumps inject non-physical oscillations in time-marching solutions. Inasmuch as the physical dependence of τ on $\dot{E}$ is believed to be less abrupt near $\dot{E} = 0$ and to approach a saturation value for $\dot{E}$ large it was decided to postulate that the dynamic inelastic constitutive function is

$$\tau_d(E,\dot{E}) = \tau_s(E) + K \tanh \beta\dot{E} \tag{6}$$

where K and β are parameters which may be adjusted to provide correlation with dynamic material tests.

The results from both the Hopkinson bar tests and the static tests have been replotted as τ_d versus $\dot{E}$ in Figure 5 in order to facilitate a graphical fitting of the surface defined by Equation (6). Each dynamic test covers a range of strains E (and of strain rate $\dot{E}$) but the results are too eratic to permit construction of curves of E = constant. Values of K and β were determined initially when only the "open-loop" data were available (Fit I). When the additional data shown in the "hatched loops" was provided a second evaluation of the parameters was made (Fit II). Both sets of parameters are listed in Table 1.

TABLE 1. STRAIN-RATE PARAMETERS

Fit	K(MPa)	K(psi)	β(s)
I	64.8	9392	0.008069
II	126.7	18370	0.003604

Curves corresponding to these fits are indicated in Figure 5 for $\tau_s(0.08)$. For other values of τ_s these curves would shift vertically.

The matter of implementing the constitutive function of Equation (6) in a response code which employs the mechanical sublayer model has been investigated. In this model

$$\tau_s(E) = \sum_{k=1}^{m} C_k \tilde{\tau}_k(E) \tag{7}$$

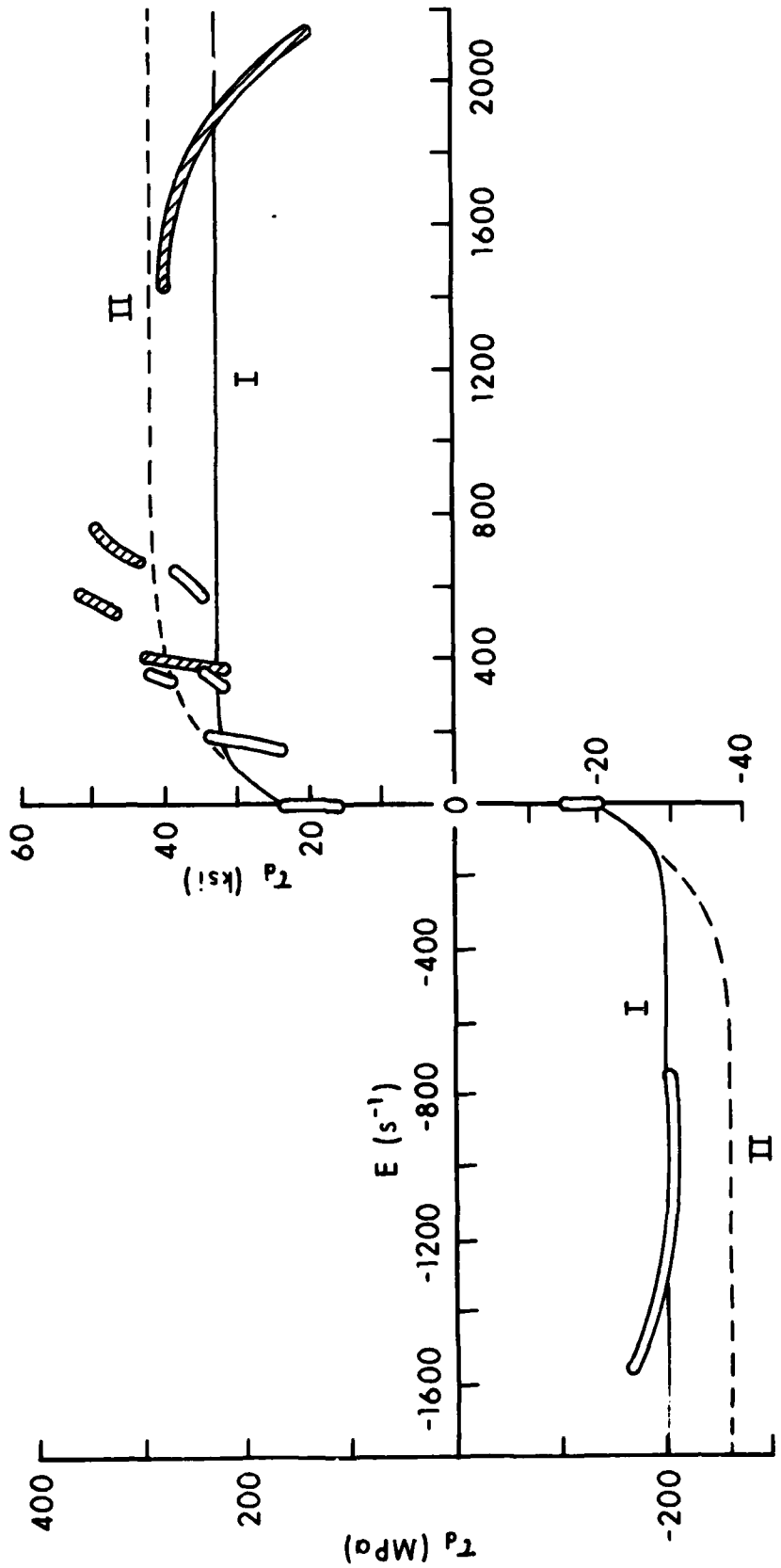

Figure 5. Stress vs strain-rate data for 3003 aluminum alloy.

the total stress τ_s at a material point is obtained as a weighted average of the stresses $\tilde{\tau}_k$ in m hypothetical elastic, perfectly plastic sublayers, all of which are at the same strain E. Each sublayer has a distinct yield stress $\tilde{\tau}_{0k}$. The C_k are the appropriate weighting factors. If the rate-dependent stresses are to be determined using a similar expression

$$\tau_d(E,\dot{E}) = \sum_{k=1}^{m} C_k \hat{\tau}_k(E,\dot{E}) \tag{8}$$

with the same weighting factors C_k then it is necessary to take the yield stress of the first sublayer to be

$$\hat{\tau}_{01}(\dot{E}) = \tilde{\tau}_{01} + \frac{K}{C_1} \tanh \beta\dot{E} \tag{9}$$

and the remaining sublayer yield stresses to be

$$\hat{\tau}_{0k} = \tilde{\tau}_{0k} \qquad \text{for} \qquad k > 1 \tag{10}$$

III. FRICTION AND ROTATORY INERTIA MODELING

Since it was desired that the beam specimens be tested with simply supported ends, CEL had designed and fabricated rocker shafts which supported the ends of the test specimens and which in turn were supported in split bearing blocks. Had these shafts been massless and had all rubbing surfaces been frictionless this design should have provided a good simulation of the desired boundary conditions (mathematically specified as no transverse displacement and no bending moment at either end of the beam). However, in view of the cited discrepancies between predictions for response of simply supported beams and the experimental data it was decided that the effects of imperfect boundary condition simulation should be evaluated. In an effort to avoid large membrane forces in the beams when finite deflections occur, the test fixture had been designed to permit one end of the beam of slide through its rocker shaft. Owing to this lack of symmetry of the boundary conditions a separate formulation was developed for each boundary.

A. Formulation for the Pinned End Condition

One end of each beam specimen was bolted to its rocker shaft with a pair of force transducers sandwiched between the lower surface of the beam and the attachment surface of the shaft. This end of the beam could only rotate, no translation being permitted in either the transverse or longitudinal direction. A drawing showing details of the pinned end rocker shaft is included as Figure 6. Free body diagrams showing the forces and moments acting on the rocker shaft and on the end segment of the beam are presented in Figure 7. The symbols have the following definitions:

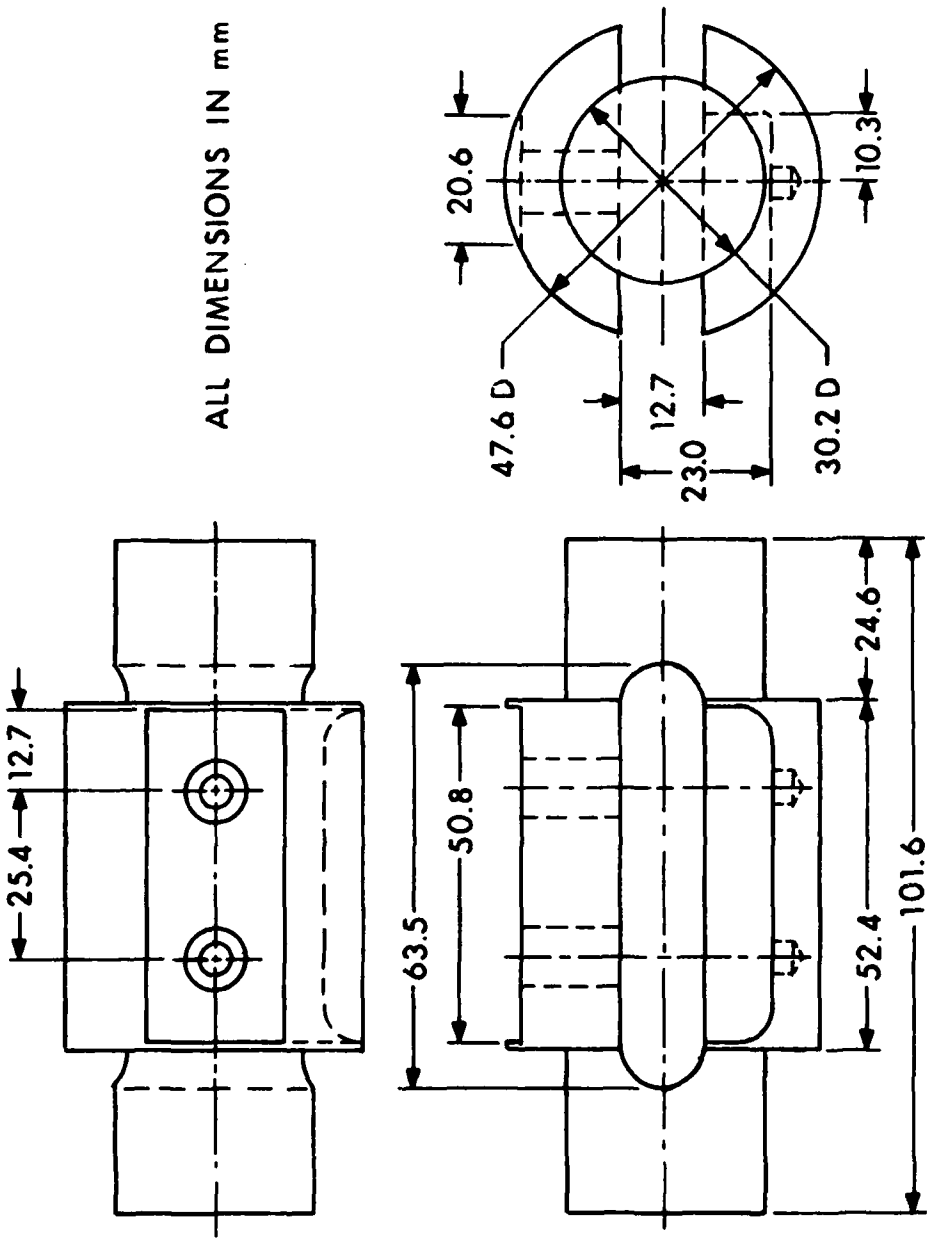

Figure 6. Pinned end rocker shaft details.

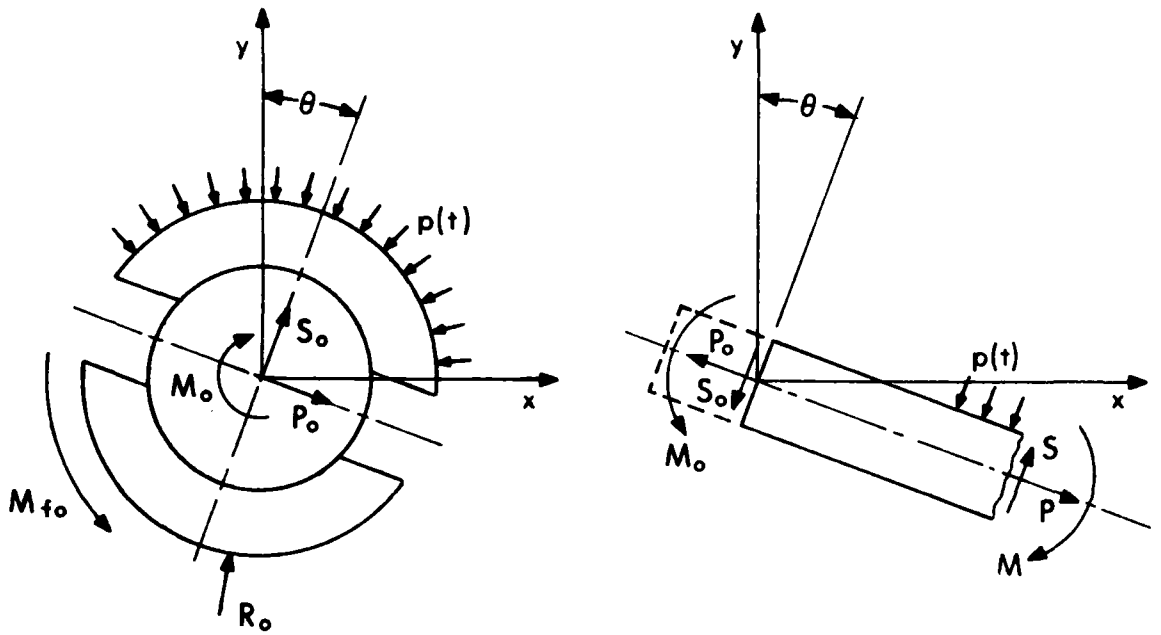

(a) Rocker Shaft

(b) Beam Segment

Figure 7. Free body diagrams at pinned end.

θ = angle of rotation of rocker shaft and of normal to beam reference surface at x = 0.

$p(t)$ = blast pressure loading

P_0 = membrane force in beam at x = 0.

S_0 = transverse shear force in beam at x = 0.

M_0 = bending moment in beam at x = 0.*

R_0 = reactive force of bearing blocks on rocker shaft.

M_{f0} = frictional moment acting at bearing interface.

A = projected area of rocker shaft surface on which blast pressure acts.

e = radius of bearing

μ = coefficient of Coulomb friction.

The equilibrium equations for the rocker shaft are

$$P_0 \cos\theta + S_0 \sin\theta + R_{0x} = 0 \tag{11}$$

$$-P_0 \sin\theta + S_0 \cos\theta + R_{0y} - pA = 0 \tag{12}$$

where R_{0x}, R_{0y} are the x- and y- components of R_0. These components can be combined to obtain

$$\begin{aligned} R_0 &= \sqrt{R_{0x}^2 + R_{0y}^2} \\ &= \left[P_0^2 + S_0^2 + 2pA\,(P_0 \sin\theta - S_0 \cos\theta) + p^2A^2\right]^{\frac{1}{2}} \end{aligned} \tag{13}$$

The frictional moment can then be determined using

$$\begin{aligned} M_{f0} &= \mu e\, R_0\, C(\dot{\theta}) \\ &= \mu e\, C(\dot{\theta})\left[P_0^2 + S_0^2 + p^2A^2 + 2pA\,(P_0 \sin\theta - S_0 \cos\theta)\right]^{\frac{1}{2}} \end{aligned} \tag{14}$$

The small "overhang" of the beam is neglected except for its contribution to the moment of inertia of the rocker assembly.

where $C(\dot{\theta})$ is the nonlinear function which may be represented graphically as indicated and which presently will be formulated analytically.

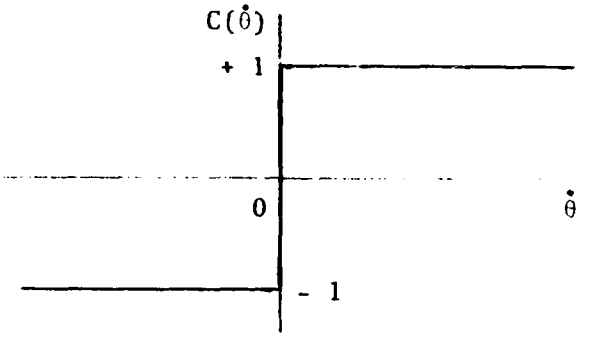

The rotational equation of motion from the free body diagram of Figure 7(a) is

$$M_0 - M_{f0} = I_0\ddot{\theta} \tag{15}$$

where I_0 is the mass moment of inertia of the material which rotates with the angular acceleration $\ddot{\theta}$. This ordinary differential equation may be replaced by the customary $O(\Delta t^2)$ central difference approximation consistent with the time integration algorithm employed in the REPSIL code. Letting

$$\Delta\theta^+ = \theta(t_{j+1}) - \theta(t_j) \tag{16}$$

$$\Delta\theta^- = \theta(t_j) - \theta(t_{j-1}) \tag{17}$$

where

$$t_{j+1} = t_j + \Delta t, \tag{18}$$

Equation (15) may be re-expressed as

$$\Delta\theta^+ = \Delta\theta^- + \frac{(\Delta t)^2}{I_0}(M_{0,j} - M_{f0,j}) \tag{19}$$

By use of Equation (19) a discrete numerical solution for $\theta(t)$ can be obtained concurrently with the marching out of the solution for the beam response. The initial conditions for $\theta(t)$ are $\theta(0) = 0$ and $\dot{\theta}(0) = 0$. In utilizing Equation (14) to obtain the value of $M_{f0,j}$ to employ in Equation (19), one must determine the value of $C(\dot{\theta})$ in accordance with one of the following three possibilities:

1. $\dot{\theta} > 0$ or $(\dot{\theta} = 0, \ddot{\theta} > 0)$ for which $C(\dot{\theta}) = +1$
2. $\dot{\theta} = 0$, $\ddot{\theta} = 0$ for which $-1 < C(\dot{\theta}) < 1$ and $M_{f0} = M_0$

3. $\dot{\theta} < 0$ or $(\dot{\theta} = 0, \ddot{\theta} < 0)$ for which $C(\dot{\theta}) = -1$

Although somewhat awkward in appearance, these tests to determine which regime is operative can be readily programmed into the time marching algorithm of the response code.

B. Formulation for the Sliding-Hinged End Condition

The support condition at the other end of the beam is similar to that at the pinned end in that the rocker shaft (see Figure 8) does not translate but is complicated by the provision for the beam to slide through the slot in the rocker shaft as the lateral displacement of the beam varies. The formulation of the boundary conditions at this end of the beam entails the introduction of two additional dependent variables:

ψ = angle of rotation of the rocker shaft

u = displacement of point in beam initially on axis of rocker shaft parallel to sliding interface

Other symbols employed in this formulation are:

S_N = transverse shear force in beam at x = N.

F_f = frictional force at sliding interface

M_T = moment transmitted between beam and rocker shaft

M_{fN} = frictional moment acting at bearing interface

R_N = reactive force of bearing blocks on rocker shaft

B = projected area of rocker shaft surface upon which blast pressure acts

m = mass of beam considered in free body diagram, including overhang material

h = depth of beam

Referring to Figure 9(a), we may write the equation of motion for the direction parallel to the sliding surface as

$$-P + F_f = m\ddot{u} \tag{20}$$

where it is tacitly assumed that the angular velocity of the rocker shaft is never large enough that a distinction between relative and absolute acceleration of m is necessary. Defining incremental changes in u in the same manner as for θ, Equation (20) may be expressed in finite difference form as

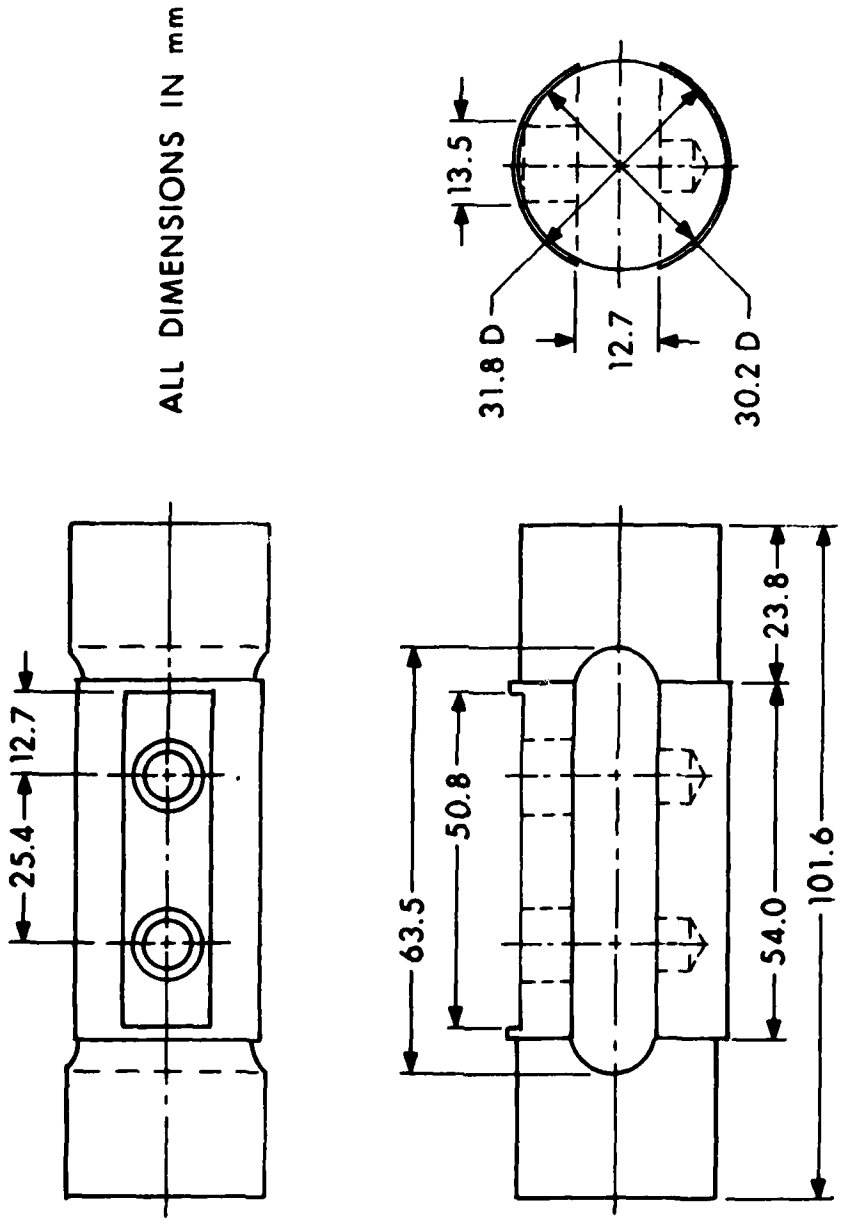

Figure 8. Sliding-hinged end rocker shaft details.

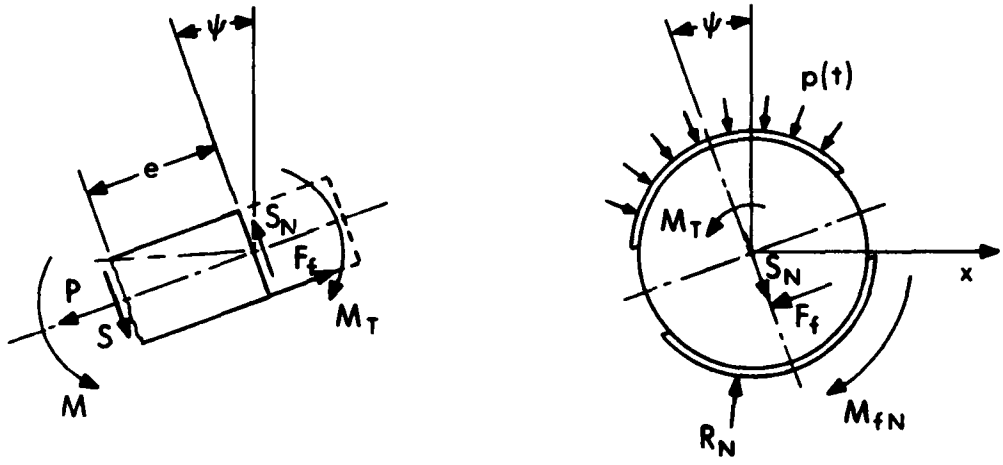

(a) Beam Segment (b) Rocker Shaft

Figure 9. Free body diagrams at sliding-hinged end.

$$\Delta u^{+} = \Delta u^{-} + \frac{(\Delta t)^2}{m} (-P + \mu S_n C(\dot{u})) \tag{21}$$

Since the REPSIL code employs Cartesian components of displacement increments, these can be obtained for the mesh location initially on the rocker shaft axis by use of

$$\Delta u_x = -\Delta u \cos \psi \tag{22}$$

$$\Delta u_y = -\Delta u \sin \psi \tag{23}$$

Also with respect to Figure 9(a) we may write the moment equation

$$M - M_T + Se + \frac{h}{2} F_f = I_B \ddot{\psi} \tag{24}$$

where I_B is the centroidal moment of inertia of m.

For the rocker shaft (see Figure 9(b)) we obtain the following equations of equilibrium and of motion:

$$-F_f \cos \psi + S_N \sin \psi + R_{Nx} = 0 \tag{25}$$

$$-F_f \sin \psi - S_N \cos \psi + R_{Ny} - pB = 0 \tag{26}$$

$$M_T - M_{fN} - \frac{h}{2} F_f = I_s \ddot{\psi} \tag{27}$$

Making use of Equations (25) and (26) the bearing reaction is obtained:

$$\begin{aligned} R_N &= \sqrt{R_{Nx}^2 + R_{Ny}^2} \\ &= [F_f^2 + S_N^2 + p^2B^2 + 2pB (F_f \sin \psi + S_N \cos \psi)]^{\frac{1}{2}} \end{aligned} \tag{28}$$

The frictional moment at the bearing is then

$$\begin{aligned} M_{fN} &= \mu e R_N C(\dot{\psi}) \\ &= \mu e C(\dot{\psi}) [F_f^2 + S_N^2 + p^2B^2 + 2pB (F_f \sin \psi + S_N \cos \psi)]^{\frac{1}{2}} \end{aligned} \tag{29}$$

Adding Equation (24) to Equation (27), one obtains

$$M - M_{fN} + Se = I_N \ddot{\psi} \tag{30}$$

where $I_N = I_s + I_B$ is the mass moment of inertia of the shaft and the contained beam.

Equation (30) may be expressed as the difference equation

$$\Delta\psi^{+} = \Delta\psi^{-} + \frac{(\Delta t)^2}{I_N} (M_{N,j} - M_{fN,j} + e\, S_{N,j}) \tag{31}$$

The formulation of the boundary conditions for the sliding-hinged end contains the two Coulomb functions $C(\dot{u})$, $C(\dot{\psi})$ which must be evaluated by tests analogous to those prescribed for $C(\dot{\theta})$; i.e., the possibilities of forward slip, no slip, or reverse slip must be considered at each sliding interface.

The foregoing boundary condition formulations, which take account of boundary friction and the rotatory inertias of boundary masses, have been incorporated into the REPSIL code as a temporary modification in order to perform an evaluation of the contribution of each of these effects.

IV. APPLICATION OF THE GENERALIZED RESPONSE ANALYSIS

All calculations to be reported in sequel pertain to the case identified as Shot Number 5 in Reference 1. The beam specimen had a rectangular cross section, 5.08 cm (2 in.) wide by 1.11 cm (7/16 in.) deep, and a span of 30.48 cm (12 in.); it was fabricated from 3003 aluminum alloy. Static tensile stress-strain data for this material were reported in Figure A-2 of Reference 1. The blast loading, assumed uniformly distributed spatially, was the experimentally recorded pressure history shown in Figure 48 of the same reference. Other input parameters used in the calculations are:

$A = 2419\ mm^2\ (3.75\ in^2)$

$B = 1452\ mm^2\ (2.25\ in^2)$

$C = 15.1\ mm\ (0.594\ in)$

$I_0 = 0.15325\ g{\cdot}m^2\ (0.0013564\ lb{\cdot}in{\cdot}s^2)$

$I_N = 0.05360\ g{\cdot}m^2\ (0.0004744\ lb{\cdot}in{\cdot}s^2)$

$m = 0.0303\ kg\ (0.0001728\ lb{\cdot}s^2/in)$

The computer runs of the REPSIL code which were made for correlation with the experimental data for Shot Number 5 are listed in Table 2. A comparison of transient mid-span deflections for each run is shown in Figure 10 as well as the experimental final value of this quantity (unfortunately, the transient experimental data were lost). Damping was initiated in each run after the maximum displacement in order to obtain a predicted final deflection, which is listed in Table 2. Runs A, B, and C were reported in Reference 1 and are included for completeness. It is clear that use of simply supported end conditions (run A) results in a gross overprediction of the response. On the other hand, runs B and C which were made using fixed end conditions effectively bracket the experimental final deflection. However, run C employed

TABLE 2. EXPERIMENTAL/THEORETICAL CORRELATIONS FOR SHOT NO. 5

ITEM	CONSTITUTIVE MODEL	BOUNDARY CONDITIONS	FRICTION COEFFICIENT	MAXIMUM DEFLECTION (mm)	FINAL DEFLECTION (mm)	MAXIMUM STRAIN AT			MAXIMUM TRANSVERSE SHEAR AT PINNED END (N)
						16.2%Span	43.3%Span	82.3%Span	
Exp. Data				----	11.2	.0020	.0152	.0025	15570
Run A	EP-SH	Simply Supp.		54.6	45.7	.0036	.0598	.0034	6310
Run B	EP-SH	Fixed		15.4	12.6	.0018	.0186	.0023	10160
Run C	EP-SH-PLSR	Fixed		13.6	10.8	.0014	.0172	.0017	10342
Run D	EP-SH-HTSR-I	Fixed		14.3	11.4	.0014	.0182	.0016	10008
Run E	EP-SH	RM+F	0.5	37.9	32.2	.0022	.0311	.0023	7673
Run F	EP-SH	RM+F	1.0	28.2	21.7	.0018	.0232	.0022	7962
Run G	EP-SH-HTSR-I	RM+F	1.0	26.8	20.4	.0017	.0211	.0022	7985
Run H	EP-SH-HTSR-II	RM+F	1.0	26.8	20.5	.0017	.0211	.0022	7985
Run I	EP-SH-HTSR-I	0.1 RM+F	1.0	28.2	22.2	.0016	.0210	.0021	8007
Run J	EP-SH-HTSR-I	RM+F	2.0	16.7	12.8	.0012	.0186	.0016	7985
Run K	EP-SH-HTSR-I	RM+F	3.0	15.6	11.8	.0012	.0176	.0012	7985

Constitutive Model abbreviations:

EP-SH	Elastoplastic strain-hardening
PLSR	Power law strain-rate dependence
HTSR	Hyperbolic tangent strain-rate dependence
I & II	Data fits defined in Table 1

Boundary condition abbreviation:

RM+F	Rotating masses plus friction (model formulated in Chapter III)

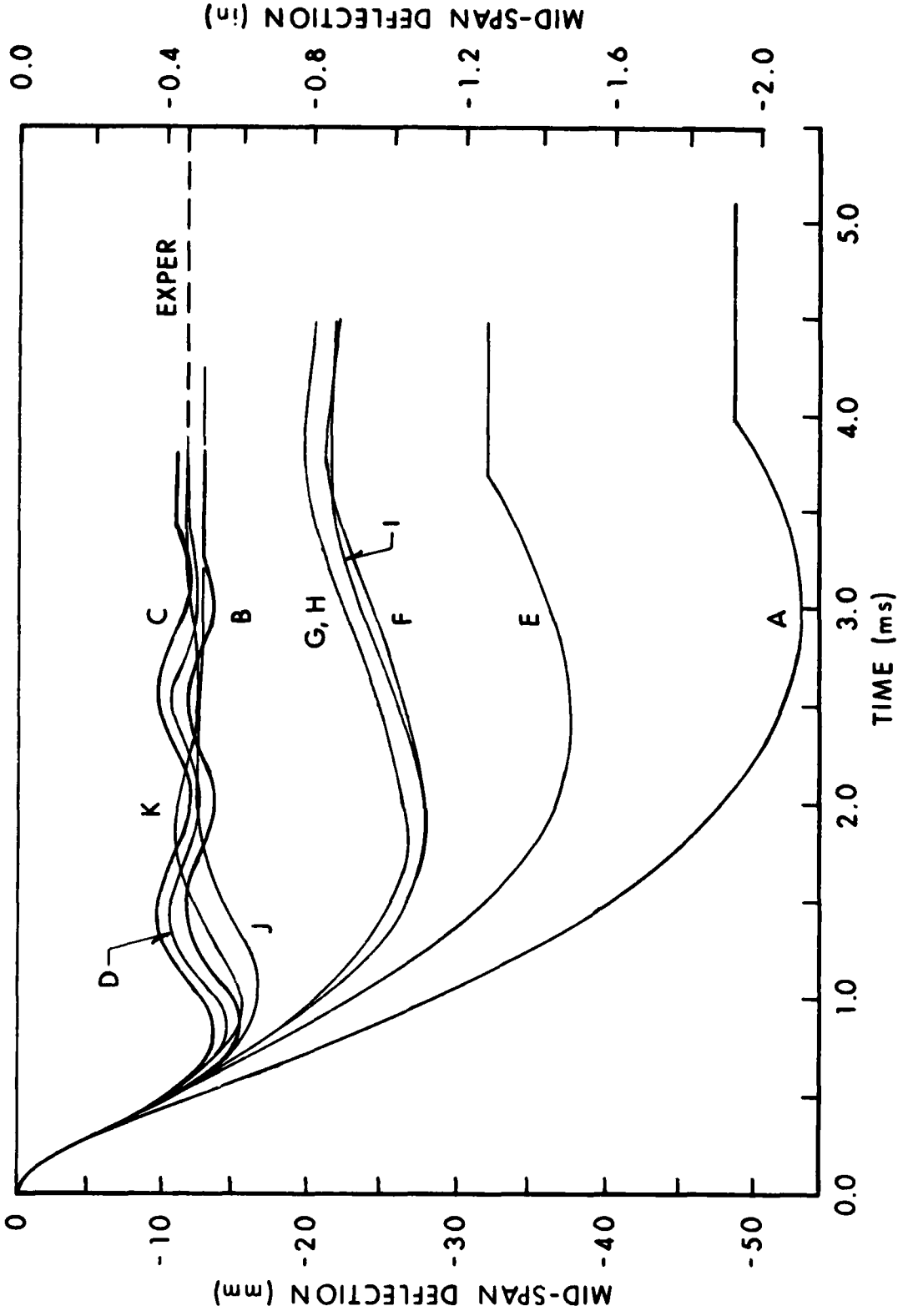

Figure 10. Comparison of deflection responses for Shot 5.

the power law strain-rate model of Equation (4) with parameters for a different aluminum alloy. When dynamic data for 3003 aluminum alloy became available the parameters of Fit I given in Table 1 were used with the hyperbolic tangent strain-rate model of Equation (6) to make run D, also with fixed boundaries. This run provided excellent agreement with the experimental final deflection. However, it was realized that the physical response did involve rotation of the rocker shafts and slippage of one end of the beam through the slotted rocker shaft so a more rational response modeling was sought.

The remaining REPSIL runs employed the boundary condition formulations developed in Chapter III. Runs E and F were made using static material properties (no strain-rate dependence in the constitutive function) and illustrate the dominant effect of the friction coefficient μ on the response. Run G was then made using the same value of μ as Run F but employing the hyperbolic tangent strain-rate model and the data of Fit I. As may be seen from Figure 10, the inclusion of strain-rate dependence had a relatively small effect in this instance, amounting to a further decrease in the final deflection of 12% of the experimental value. When Fit II was effected, Run H was made using these material properties and the same value of μ; the results were essentially identical to those of run G. This somewhat surprising indifference to the strain-rate data fitting has the following explanation. For Shot No. 5 the maximum strain rate calculated was only $120.8 s^{-1}$ at one location in the beam and for most of the response the strain-rate was much less throughout the beam. Referring to Figure 5, one sees that there is no significant difference between Fits I and II for such small strain-rates. Conversely, for stronger blasts which induce higher strain-rates one could expect that the difference between solutions using Fits I and II would be significant.

It is instructive to examine certain other results produced by the REPSIL program for Run G (to which results for other runs are qualitatively similar). Figure 11 shows the variation of the bending moment M_0 and the frictional moment M_{f0} at the pinned end while Figure 12 displays the transient rotation of the rocker shaft at the same location. It may be seen that no rotation occurs until about 0.23 ms when M_{f0} is no longer able to match M_0. Subsequently the end of the beam rotates until about 1.81 ms when the shaft "locks up" ($M_{f0} = M_0$) and θ remains constant until the reversed bending moment becomes large enough to overcome the frictional resistance. Another brief period of ankylosis starts at about 4.13 ms. The predicted transient behavior of the transverse shear force at the pinned end of the beam is presented in Figure 13. It should be observed that the maximum magnitude of this shear reaction occurs before the end of the beam starts to rotate. However, prior to this the material at this location experiences inelastic deformation. No explanation for the discrepancy between predicted values of this quantity and the experiment value is feasible since the experimental value is 50% greater than that which would be expected if the boundary condition were total fixity.

It was desired to assess the importance of including the rotatory inertia of the end masses in the response formulation. This cannot be accomplished by simply making a run with the mass moments of inertia I_0 and I_N set equal to zero (see Equations (19) and (31)). Rather than program a special formulation

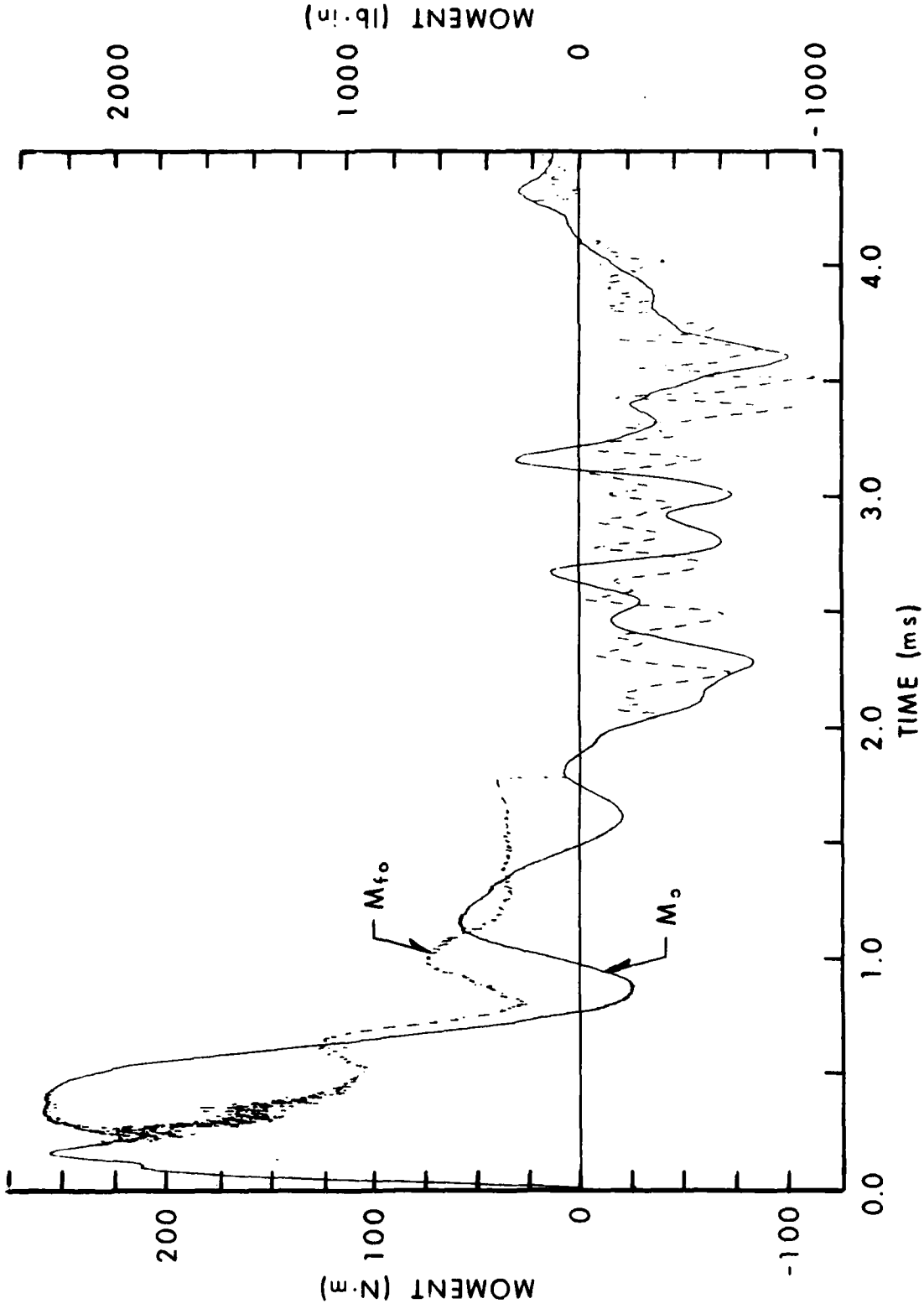

Figure 11. Transient moments at pinned end.

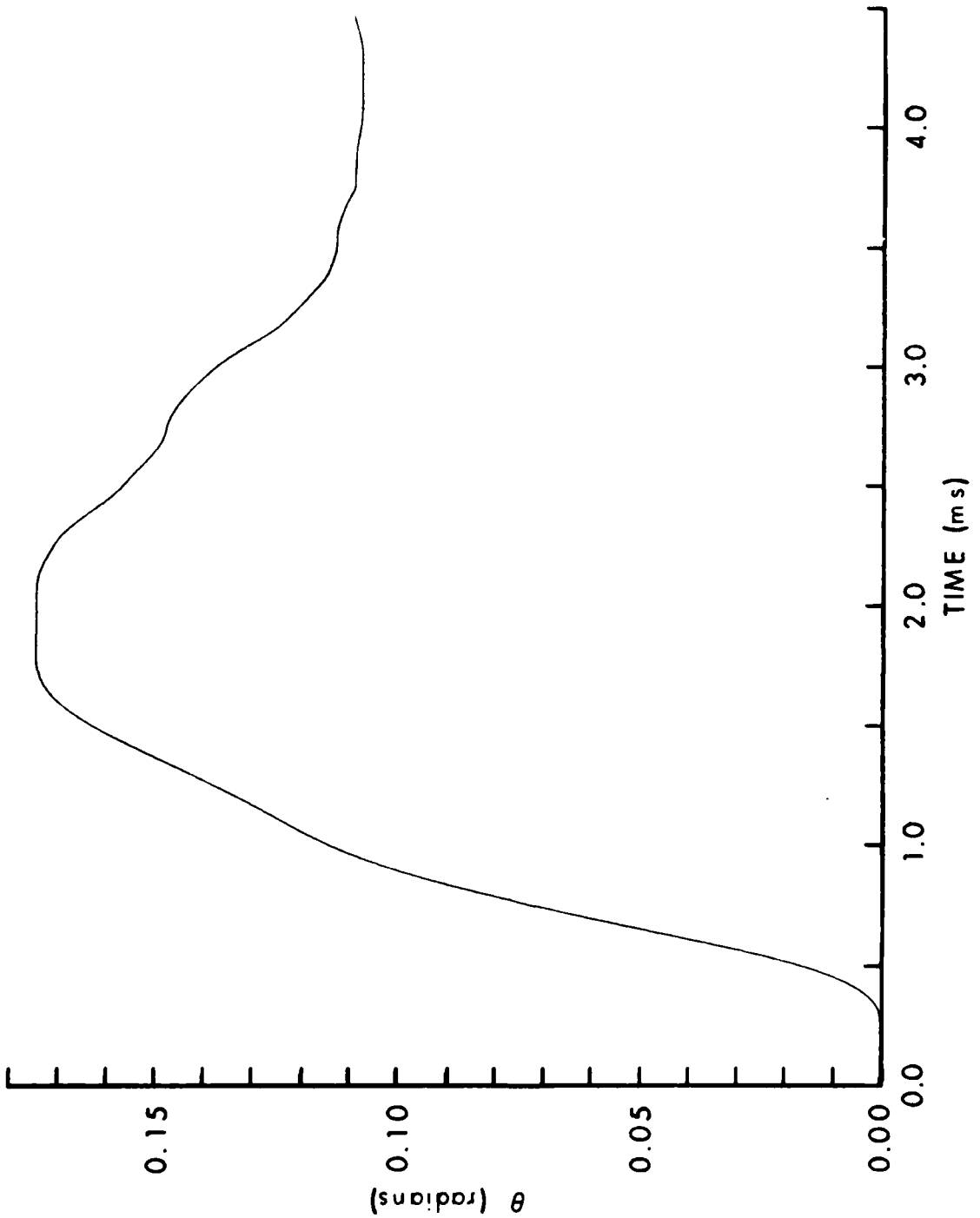

Figure 12. Predicted rotation at pinned end.

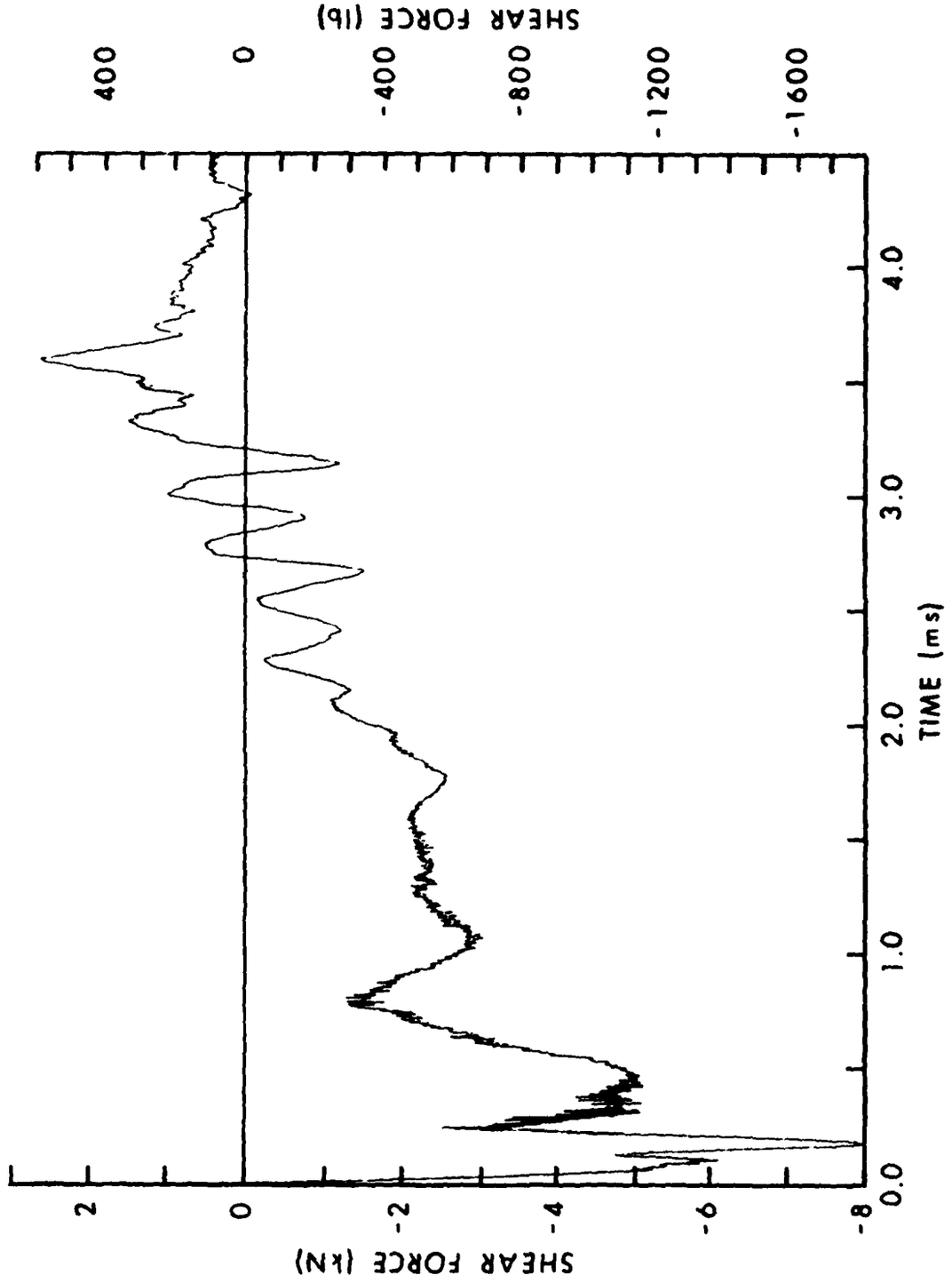

Figure 13. Transverse shear reaction at the pinned end.

for this case, the available program was used with the values of I_0 and I_N set to a small fraction of their actual values. This was done in Run I where the fraction employed was 1/10. The results should be compared with Run G since all other parameters were the same for these two runs. It may be seen from Figure 10 that the form of the response curve is somewhat altered for Run I. The final displacement is about 16% (of the experimental value) greater when the rotatory inertia effect is minimized.

Since none of the cases examined for $\mu = 1$ resulted in a final displacement approximating the experimental value it was decided to explore further the effect of varying this parameter. This was done in Runs J and K using $\mu = 2$ and 3 respectively. Run K provided a very satisfactory correlation with respect to final deflections. In fact, further increase in μ would have little effect since, even for Run K, the end masses were "locked" during most of the run. The use of such large values of friction coefficient may seem inappropriate but there is essentially no data on Coulomb friction under conditions where both the driving force and the normal pressure are rapidly changing.

It is observed that strains, both experimental and analytical, vary directly with the transverse displacement amplitude. Thus, the best correlations with experimental strain data occur for runs which best match the experimental final deflection.

V. CONCLUSIONS

The foregoing analytical formulations for strain-rate effects plus friction and rotatory inertia at supports have permitted a more rational interpretation of experimental data from blast loaded beam tests reported in Reference 1. Through use of selective computer runs of modified REPSIL code it was possible to evaluate the relative importance of each of these effects on the overall response.

The 3003 aluminum alloy used in fabricating the beam specimens was determined by Hopkinson bar experiments to be significantly more strain-rate sensitive than most structural aluminum alloys. The use of the hyperbolic tangent function strain-rate model introduced in this report is believed preferable to the widely used power law model due to its more realistic behavior for small strain rates. Inclusion of strain-rate effects in the response calculations for Shot 5 produced only a small change in beam deflection due to the rather small strain-rates which were associated with this shot. One should not conclude that strain-rate effects are always insignificant; for problems where strain-rates in the saturation region occur for an appreciable portion of the response, resisting stress increases of 40% and 78% would be available for Fits I and II, respectively.

Although the intended simply supported end conditions for the beam tests were not achieved experimentally the boundaries were certainly not completely fixed. The augmentation of REPSIL boundary conditions to account for support friction and rotatory inertia permitted the determination that the observed response was primarily due to large frictional forces at the boundaries. The relatively small effect of the rotatory inertia of the rocker shafts did alter

the mathematical character of the problem and provided a smoothing effect on the response calculations.

A motivating consideration for performing the cited beam tests had been to establish the existence of large transient shears near the ends of blast-loaded simply supported beams.[6] The presence of such shears could necessitate a revision of statics-based design procedures for beams and slabs. Calculations for all boundary conditions used in this investigation indicate that such shears are present and this is consistent with the test data. However, unlike the simply supported beam problem in which bending is insignificant where the shears are large, for fixed or "locking" ends the region near the ends of the beam is subjected simultaneously to large bending and shearing stresses. Therefore, design procedures for beams with constrained ends must consider the dynamic combined stress states which will be present.

[6] *W. A. Keenan, "Shear Stress in One-Way Slabs Subjected to Blast Load," Civil Engineering Laboratory Technical Memorandum No. M-51-77-10, August 1977.*

REFERENCES

1. C. N. Kingery, N. J. Huffington, Jr., and J. D. Wortman, "Response of Beams to Airblast Loading," Ballistic Research Laboratory Technical Report ARBRL-TR-02369, September 1981.(AD B060635L)

2. J. D. Wortman, "RPSL1D (A One-Dimensional Version of REPSIL)," Ballistic Research Laboratory Memorandum Report ARBRL-MR-03221, November 1982. (AD A122336)

3. Private communications from S. J. Bless and A. Challita, UDRI to N. J. Huffington, Jr., BRL.

4. S. J. Bless, A. Challita, and A. M. Rajendran, "Dynamic Tensile Test Results for Several Metals," Air Force Material Laboratory Report AFWAL-TR-82-4026, April 1982.

5. P. S. Symonds, "Viscoplastic Behavior in Response of Structures to Dynamic Loading," in Behavior of Materials Under Dynamic Loading, N. J. Huffington, Jr., Editor, ASME, 1965.

6. W. A. Keenan, "Shear Stress in One-Way Slabs Subjected to Blast Load," Civil Engineering Laboratory Technical Memorandum No. M-51-77-10, August 1977.

DISTRIBUTION LIST

No. of Copies	Organization
12	Administrator Defense Technical Info Center ATTN: DTIC-DDA Cameron Station Alexandria, VA 22314
4	Director of Defense Research and Engineering ATTN: DD/TWP DD/S&SS DD/I&SS AD/SW Washington, DC 20301
2	Asst. to the Secretary of Defense (Atomic Energy) ATTN: Document Control Donald R. Cotter Washington, DC 20301
3	Director Defense Advanced Research Projects Agency ATTN: Tech Lib NMRO PMO 1400 Wilson Boulevard Arlington, VA 22209
2	Director Federal Emergency Management Agency ATTN: Mr. Michael Pachuta/RF-SR Technical Library Washington, DC 20472
4	Director Defense Intelligence Agency ATTN: DT-1B DB-4C/E. O. Farrell DT-2/Wpns & Sys Div RDS-344 Washington, DC 20301
1	Director National Security Agency ATTN: E. F. Butala, R15 Ft. George G. Meade, MD 20755
3	Director Joint Strategic Target Planning Staff JCS ATTN: Sci & Tech Info Lib JLTW-2 DOXT Offut AFB, NB 68113
1	Director Defense Communications Agency ATTN: Code 930 8th St & S. Courthouse Road Washington, DC 20305
5	Director Defense Nuclear Agency ATTN: STSI/Archives SPAS STSP STVL/Dr. La Vier RATN Washington, DC 20305
6	Director Defense Nuclear Agency ATTN: DDST/Dr. Conrad STTL/Tech Lib (2 cys) SPSS/K. Goering G. Ullrich SPTD/T. Kennedy Washington, DC 20305
2	Commander Field Command, DNA ATTN: FCPR FCTMOF Kirtland AFB, NM 87117
1	Commander Field Command, DNA Livermore Branch ATTN: FCPRL P.O. Box L-395 Livermore, CA 94550

DISTRIBUTION LIST

No. of Copies	Organization
1	Director Institute for Defense Analyses ATTN: IDA Librarian 1801 Beauregard Street Alexandria, VA 22311
1	Director US Army BMD Program Office ATTN: John Shea 5001 Eisenhower Avenue Alexandria, VA 22333
2	Director US Army BMD Advanced Technology Center ATTN: CRDABH-X, CRDABH-S P.O. Box 1500 Huntsville, AL 35807
1	Commander US Army BMD Systems Command ATTN: BMDSC-TFN/N. J. Hurst P.O. Box 1500 Huntsville, AL 35807
2	Deputy Chief of Staff for Operations and Plans ATTN: Technical Library Director of Chemical & Nuclear Operations Department of the Army Washington, DC 20310
2	Office, Chief of Engineers Department of the Army ATTN: DAEN-MCE-D DAEN-RDM Washington, DC 20314
1	FTD (TDPMG) Wright-Patterson AFB Ohio 45433
1	FTD (TD/BTA/Lib) Wright-Patterson AFB Ohio 45433

No. of Copies	Organization
5	Commander US Army Engineer Waterways Experiment Station ATTN: Technical Library William Flathau John N. Strange Guy Jackson Leo Ingram P.O. Box 631 Vicksburg, MS 39181
1	Commander US Army Engineering Center ATTN: ATSEN-SY-L Fort Belvoir, VA 22060
1	Division Engineer US Army Engineering Division ATTN: HNDSE-R/M.M. Dembo Huntsville Box 1600 Huntsville, AL 35804
1	Division Engineer US Army Engineering Division Ohio River ATTN: Docu Cen P.O. Box 1159 Cincinnati, OH 45201
2	HDQA (DAMA-AR, NCL Div) Washington, DC 20310
1	Commander US Army Materiel Development and Readiness Command ATTN: DRCDMD-ST 5001 Eisenhower Avenue Alexandria, VA 22333
1	Commander Armament R&D Center US Army AMCCOM ATTN: DRSMC-TDC(D) Dover, NJ 07801

DISTRIBUTION LIST

No. of Copies	Organization
2	Commander Armament R&D Center US Army AMCCOM ATTN: DRSMC-TSS(D) Dover, NJ 07801
1	Commander US Army Armament, Munitions and Chemical Command ATTN: DRSMC-LEP-L(R) Rock Island, IL 61299
1	Director Benet Weapons Laboratory Armament R&D Center US Army AMCCOM ATTN: DRSMC-LCB-TL(D) Watervliet, NY 12189
1	Commander US Army Aviation Research and Development Command ATTN: DRDAV-E 4300 Goodfellow Blvd. St. Louis, MO 63120
1	Director US Army Air Mobility Research and Development Laboratory Ames Research Center Moffett Field, CA 94035
1	Commander US Army Communications Rsch and Development Command ATTN: DRSEL-ATDD Fort Monmouth, NJ 07703
5	Commander US Army Electronics Research and Development Command ATTN: DELSD-L DELEW-E W. S. McAfee DELSD-EI, J. Roma DELSD-EM A. Sigismondi C. Goldy Fort Monmouth, NJ 07703
7	Commander US Army Harry Diamond Labs ATTN: Mr. James Gaul Mr. L. Belliveau Mr. J. Meszaros Mr. J. Gwaltney Mr. F. W. Balicki Mr. Bill Vault Mr. R. J. Bostak 2800 Powder Mill Road Adelphi, MD 20783
5	Commander US Army Harry Diamond Labs ATTN: DELHD-TA-L DRXDO-TI/002 DRXDO-NP DRXDO-RBH/P. Caldwell DELHD-RBA/J.Rosado 2800 Powder Mill Road Adelphi, MD 20783
1	Commander US Army Missile Command ATTN: DRSMI-R Redstone Arsenal, AL 35898
1	Commander US Army Missile Command ATTN: DRSMI-YDL Redstone Arsenal, AL 35898
2	Commander US Army Missile Command ATTN: MICOM-XS/Chief Scientist Technical Library Redstone Arsenal, AL 35898
2	Commander US Army Natick Research and Development Laboratory ATTN: DRDNA/Dr. D. Sieling DRXNM-UE Authur Johnson Natick, MA 01760

DISTRIBUTION LIST

No. of Copies	Organization
1	Commander US Army Tank Automotive Command ATTN: DRSTA-TSL Warren, MI 48090
1	Commander US Army Foreign Science and Technology Center ATTN: Rsch & Concepts Branch 220 7th Street, NE Charlottesville, VA 22901
1	Commander US Army Logistics Mgmt Ctr ATTN: ATCL-O Mr. Robert Cameron Fort Lee, VA 23801
3	Commander US Army Materials and Mechanics Research Center ATTN: Technical Library John Mescall Richard Shea Watertown, MA 02172
1	Commander US Army Research Office P.O. Box 12211 Research Triangle Park NC 27709
3	Commander US Army Nuclear & Chemical Agcy ATTN: ACTA-NAW MONA-WE Technical Library 7500 Backlick Rd, Bldg. 2073 Springfield, VA 22150
1	Commander US Army TRADOC ATTN: ATCD Fort Monroe, VA 23651
2	Director US Army TRADOC Systems Analysis Activity ATTN: LTC John Hesse ATAA-SL White Sands Missile Range NM 88002
2	Commandant US Army Infantry School ATTN: ATSH-CD-CSO-OR Fort Benning, GA 31905
1	Commander USA Combined Arms Combat Developments Activity ATTN: ATCA-CO, Mr. L. C. Pleger Fort Leavenworth, KS 66027
1	Commandant Interservice Nuclear Weapons School ATTN: Technical Library Kirtland AFB, NM 87117
1	Chief of Naval Materiel ATTN: MAT 0323 Department of the Navy Arlington, VA 22217
2	Chief of Naval Operations ATTN: OP-03EG OP-985F Department of the Navy Washington, DC 20350
1	Office of Naval Research ATTN: N. Perrone 800 N. Quincy Street Arlington, VA 22217
3	Director Strategic Systems Projects Ofc. ATTN: NSP-43, Tech Lib NSP-273 NSP-272 Munitions Bldg, Rm 3245 Washington, DC 20360

DISTRIBUTION LIST

No. of Copies	Organization
1	Commander Naval Electronic Systems Com ATTN: PME 117-21A Washington, DC 20360
3	Commander Naval Facilities Engineering Command ATTN: Code 03A Code 04A Technical Library Washington, DC 20360
3	Commander Naval Sea Systems Command ATTN: SEA-62R SEA-62Y, SEA-9961 Department of the Navy Washington, DC 20360
7	Officer-in-Charge (Code L31) Civil Engineering Laboratory Naval Constr Btn Ctr ATTN: Stan Takahashi R. J. Odello Bill Keenan (4 cys) Technical Library Port Hueneme, CA 93041
1	Commander David W. Taylor Naval Ship Research & Development Ctr ATTN: Lib Div, Code 522 Bethesda, MD 20084
1	Commander Naval Surface Weapons Center ATTN: DX-21, Library Br Dahlgren, VA 22448
3	Commander Naval Surface Weapons Center ATTN: Code WA501/Navy Nuclear Programs Office Code WX21/Tech Lib Code 240/C.J. Aronson Silver Spring, MD 20910
2	Commander Naval Weapons Center ATTN: Code 3431, Tech Lib Code 31804, M. Keith China Lake, CA 93555
2	Commander Naval Ship Research and Development Center Facility Underwater Explosions Research Division ATTN: Code 17, W. W. Murray Technical Library Portsmouth, VA 23709
2	Commander Naval Weapons Evaluation Facility ATTN: Document Control R. Hughes Kirtland AFB, NM 87117
1	Commander Naval Research Laboratory ATTN: Code 2027, Tech Lib Washington, DC 20375
1	Superintendent Naval Postgraduate School ATTN: Code 2124 Tech Reports Lib Monterey, CA 93940
1	HQ USAF (IN) Washington, DC 20330
1	HQ USAF (PRE) Washington, DC 20330
2	AFSC (DLCAW; Tech Lib)/SDOA Andrews AFB, MD 20334
2	ADTC (ADBRL-2; Tech Lib) Eglin AFB, FL 32542
2	AFATL (DLYV; P. Nash) Eglin AFB, FL 32542

DISTRIBUTION LIST

No. of Copies	Organization
1	AFATL (DLYV, Jim Flint) Eglin AFB, FL 32542
2	RADC (EMTLD/Docu Lib; EMREC/R.W. Mair) Griffiss AFB, NY 13341
1	AFWL/DE-I Kirtland AFB, NM 87117
1	AFWL/DEX Kirtland AFB, NM 87117
1	AFWL/R. Henny Kirtland AFB, NM 87117
1	AFWL/SUL, M. A. Plamondon Kirtland AFB, NM 87117
2	Commander-in-Chief Strategic Air Command ATTN: NRI-STINFO Lib SPFS Offutt AFB, NB 68113
1	AFIT (Lib Bldg. 640, Area B) Wright-Patterson AFB Ohio 45433
1	FTD (TDFBD) Wright-Patterson AFB Ohio 45433
1	Director US Bureau of Mines ATTN: Technical Library Denver Federal Center Denver, CO 80225
1	Director US Energy Research and Development Administration Albuquerque Operations Office ATTN: Document Control for Tech Lib P. O. Box 5400 Albuquerque, NM 87115

No. of Copies	Organization
1	Director Lawrence Livermore Lab ATTN: Jack Kahn/L-7 P.O. Box 808 Livermore, CA 94550
1	Director Lawrence Livermore Lab ATTN: Tech Info Dept L-3 P.O. Box 808 Livermore, CA 94550
1	Director Lawrence Livermore Lab ATTN: R. G. Dong/L-90 P.O. Box 808 Livermore, CA 94550
1	Director Lawrence Livermore Lab ATTN: Ted Butkovich/L-200 P.O. Box 808 Livermore, CA 94550
1	Director Lawrence Livermore Lab ATTN: Robert Schock/L-437 P.O. Box 808 Livermore, CA 94550
1	Director Lawrence Livermore Lab ATTN: D. Burton, L200 P.O. Box 808 Livermore, CA 94550
4	Director Los Alamos Scientific Lab ATTN: Doc Control for Rpts Lib R. A. Gentry G. R. Spillman M Davis P.O. Box 1663 Los Alamos, NM 87544
1	FTD (ETET, CPT R.C. Buscemann) Wright-Patterson AFB Ohio 45433

DISTRIBUTION LIST

No. of Copies	Organization
1	US Energy Research and Development Administration Nevada Operations Office ATTN: Doc Control for Tech Lib P.O. Box 14100 Las Vegas, NV 89114
5	Director Sandia National Laboratories ATTN: Doc Control for 3141 Sandia Rpt Collection A. M. Chaban L. J. Vortman W. Roherty L. Hill Albuquerque, NM 87115
1	Director Sandia National Laboratories Livermore Laboratory ATTN: Doc Control for Tech Lib P.O. Box 969 Livermore, CA 94550
1	Director National Aeronautics and Space Administration Scientific and Technical Information Facility P.O. Box 8757 Baltimore/Washington International Airport MD 21240
1	Aeronautical Research Associates of Princeton, Inc. ATTN: Dr. J. W. Leech P.O. Box 2229 50 Washington Road Princeton, NJ 08540
3	Aerospace Corporation ATTN: Tech Info Services (2 cys) P. N. Mathur P.O. Box 92957 Los Angeles, CA 90009
1	Agbabian Associates ATTN: M. Agbabian 250 North Nash Street El Segundo, CA 90245
1	Applied Theory, Inc. ATTN: John G. Trulio 1010 Westwood Blvd Los Angeles, CA 90024
1	Artec Associates, Inc. ATTN: Steven Gill 26046 Eden Landing Road Hayward, GA 94545
1	AVCO Systems Division ATTN: Res Lib A830, Rm 7201 201 Lowell Street Wilmington, MA 01887
1	The BDM Corporation ATTN: Richard Hensley P.O. Box 9274 Albuquerque International Albuquerque, NM 87119
2	The Boeing Company ATTN: Aerospace Library R. H. Carlson P.O. Box 3707 Seattle, WA 98124
1	Calspan Corporation ATTN: Technical Library P.O. Box 400 Buffalo, NY 14225

DISTRIBUTION LIST

No. of Copies	Organization
1	EG&G, Incorporated Albuquerque Division ATTN: Technical Library P.O. Box 10218 Albuquerque, NM 87114
1	The Franklin Institute ATTN: Zemons Zudans 20th Street and Parkway Philadelphia, PA 19107
2	General American Trans Corp. General American Research Div ATTN: G. L. Neidhardt M. R. Johnson 7449 N. Natchez Avenue Niles, IL 60648
1	Kaman-TEMPO ATTN: DASIAC P.O. Drawer QQ Santa Barbara, CA 93102
1	The Johns Hopkins University School of Engineering ATTN: J. F. Bell Baltimore, MD 21218
1	Kaman-TEMPO ATTN: E. Bryant, Suite UL-1 715 Shamrock Road Bel Air, MD 21014
2	Hazeltine Corp. ATTN: Carl Meinen Greenlawn, NY 11740
1	J. H. Wiggins Co., Inc. ATTN: John Collins 1650 South Pacific Cost Highway Redondo Beach, CA 90277
5	Kaman AviDyne ATTN: Dr. N. P. Hobbs (4 cys) Mr. S. Criscione 83 Second Avenue Northwest Industrial Park Burlington, MA 01830
3	Kaman Sciences Corporation ATTN: Library P. A. Ellis F. H. Shelton 1500 Garden of the Gods Road Colorado Springs, CO 80907
1	Kaman Sciences Corporation ATTN: Don Sachs Suite 703 2001 Jefferson Davis Highway Arlington, VA 22202
1	Lockheed Missiles & Space Co. ATTN: Technical Library P.O. Box 504 Sunnyvale, CA 94086
1	Martin Marietta Corporation Aerospace Division ATTN: G. Fotieo P.O. Box 5837 Orlando, FL 32805
3	McDonnell Douglas Astronautics Company ATTN: Robert W. Halprin Mr. C. Gardiner Dr. P. Lewis 5301 Bolsa Avenue Huntington Beach, CA 92647
1	Meredith Engineering ATTN: D. Meredith 33170 Glen Valley Drive Farmington Hills, MI 48018
2	Merritt Cases, Inc. ATTN: J. L. Merritt Technical Library P.O. Box 1206 Redlands, CA 92373
1	Meteorology Research, Inc. ATTN: W. D. Green 454 West Woodbury Road Altadena, CA 91001

DISTRIBUTION LIST

No. of Copies	Organization
1	The Mitre Corporation ATTN: Library P.O. Box 208 Bedford, MA 01730
1	Old Dominion University Dept. of Mechanical Engineering and Mechanics ATTN: Dr. E. T. Kruszewski Norfolk, VA 23508
1	Pacific Sierra Research Corp ATTN: Dr. Harold Brode 1456 Cloverfield Boulevard Santa Monica, CA 90404
2	Pacifica Technology ATTN: G. Kent R. Bjork P.O. Box 148 Del Mar, CA 92014
5	Physics International Corp ATTN: Robert Swift Charles Godfrey Larry A. Behrmann Fred Sauer Technical Library 2700 Merced Street San Leandro, CA 94577
3	R&D Associates ATTN: Dr. Albert L. Latter William B. Wright A. Kuhl P.O. Box 9695 Marina del Rey, CA 90291
3	R&D Associates ATTN: Jerry Carpenter J. G. Lewis Tech Library P.O. Box 9695 Marina del Rey, CA 90291
1	R&D Associates Suite 500 1851 N. Ft. Myer Drive Arlington, VA 22209
1	AFELM, The Rand Corporation ATTN: C. C. Mow 1700 Main Street Santa Monica, CA 90406
2	Science Applications, Inc. ATTN: Bert Chambers John Cockayne 1710 Goodridge Drive, PO Box 1303 McLean, VA 22102
1	Science Applications, Inc. 2450 Washington Avenue Suite 120 San Leandro, CA 94577
2	Science Applications, Inc. ATTN: Technical Library Michael McKay 1250 Prospect Plaza La Jolla, CA 92037
1	Systems Science and Software ATTN: C. E. Needham P.O. Box 8243 Albuquerque, NM 87108
4	Systems Science and Software ATTN: Donald R. Grine Ted Cherry Thomas D. Riney Technical Library P.O. Box 1620 La Jolla, CA 92037
3	Terra Tek, Inc. ATTN: Sidney Green A. H. Jonas Technical Library 420 Wakara Way Salt Lake City, UT 84108
2	Tetra Tech, Inc. ATTN: Li-San Hwang Technical Library 630 North Rosemead Blvd Pasadena, CA 91107

DISTRIBUTION LIST

No. of Copies	Organization
7	TRW Systems Group ATTN: Paul Lieberman Benjamin Sussholtz Norm Lipner William Rowan Jack Farrell Pravin Bhutta Tech Info Ctr/S-1930 One Space Park Redondo Beach, CA 90278
1	TRW Systems Group ATTN: Greg Hulcher San Bernardino Operations P.O. Box 1310 San Bernardino, CA 92402
2	Union Carbide Corporation Holifield National Laboratory ATTN: Doc Control for Tech Lib Civil Defense Research Proj P.O. Box X Oak Ridge, TN 37830
1	Universal Analytics, Inc. ATTN: E. I. Field 7740 W. Manchester Blvd Playa del Rey, CA 90291
1	Weidlinger Assoc. Consulting Engineers ATTN: M. L. Baron 110 East 59th Street New York, NY 10022
1	Westinghouse Electric Co. Marine Division ATTN: W. A. Votz Hendy Avenue Sunnyvale, CA 94008
3	Battelle Memorial Institute ATTN: Technical Library R. W. Klingesmith Dr. B. D. Trott 505 King Avenue Columbus, OH 43201
1	California Institute of Technology ATTN: T. J. Ahrens 1201 E. California Blvd. Pasadena, CA 91109
2	Denver Research Institute University of Denver ATTN: Mr. J. Wisotski Technical Library 2390 S. University Blvd Denver, CO 80210
3	IIT Research Institute ATTN: Milton R. Johnson R. E. Welch Technical Library 10 West 35th Street Chicago, IL 60616
2	Lovelace Research Institute Inhalation Toxicology Rsch Inst ATTN: Asst. Dir of Research/ Robert K. Jones Technical Library P. O. Box 5890 Albuquerque, NM 87115
1	Massachusetts Institute of Technology Aeroelastic and Structures Research Laboratory ATTN: Dr. E. A. Witmer 77 Massachusetts Avenue Cambridge, MA 02139
3	Southwest Research Institute ATTN: Dr. W. E. Baker A. B. Wenzel U. S. Lindholm 8500 Culebra Road San Antonio, TX 78228
2	SRI International ATTN: Dr. G. R. Abrahamson Carl Peterson 333 Ravenswood Avenue Menlo Park, CA 94025

DISTRIBUTION LIST

No. of Copies	Organization
1	J. D. Haltiwanger Consulting Services B106a Civil Engineering Bldg 208 N. Romine Street Urbana, IL 61801
1	University of Dayton Research Institute ATTN: Dr. S. J. Bless 300 College Park Avenue Dayton, OH 45469
3	University of Delaware Dept of Mechanical and Aerospace Engineering ATTN: Dr. J. Vinson Dr. M. Taya Dr. H. B. Kingsbury Newark, DE 19711
1	University of Florida Department of Engineering Science ATTN: L. E. Malvern Gainesville, FL 32601
2	The University of New Mexico The Eric H. Wang Civil Engineering Research Facility ATTN: Larry Bickle Neal Baum University Station Box 188 Albuquerque, NM 87106
2	Virginia Polytechnic Institute and State University Department of Engineering Mechanics ATTN: D. Frederick C. W. Smith, Jr. Blacksburg, VA 24061
2	Washington State University Administration Office ATTN: Arthur Miles Hohorf George Duval Pullman, WA 99163

Aberdeen Proving Ground

Dir, USAMSAA
ATTN: DRXSY-D
DRXSY-MP, H. Cohen
Cdr, USATECOM
ATTN: DRSTE-TO-F
Cdr, CRDC, AMCCOM
ATTN: DRSMC-CLB-PA
DRSMC-CLN
DRSMC-CLJ-L

USER EVALUATION OF REPORT

Please take a few minutes to answer the questions below; tear out this sheet, fold as indicated, staple or tape closed, and place in the mail. Your comments will provide us with information for improving future reports.

1. BRL Report Number _____

2. Does this report satisfy a need? (Comment on purpose, related project, or other area of interest for which report will be used.)

_____

_____

_____

3. How, specifically, is the report being used? (Information source, design data or procedure, management procedure, source of ideas, etc.) _____

_____

_____

4. Has the information in this report led to any quantitative savings as far as man-hours/contract dollars saved, operating costs avoided, efficiencies achieved, etc.? If so, please elaborate.

_____

_____

5. General Comments (Indicate what you think should be changed to make this report and future reports of this type more responsive to your needs, more usable, improve readability, etc.) _____

_____

_____

_____

6. If you would like to be contacted by the personnel who prepared this report to raise specific questions or discuss the topic, please fill in the following information.

Name: _____

Telephone Number: _____

Organization Address: _____

_____

_____

FOLD HERE

Director
US Army Ballistic Research Laboratory
ATTN: DRSMC-BLA-S (A)
Aberdeen Proving Ground, MD 21005

NO POSTAGE
NECESSARY
IF MAILED
IN THE
UNITED STATES

OFFICIAL BUSINESS
PENALTY FOR PRIVATE USE, $300

BUSINESS REPLY MAIL
FIRST CLASS PERMIT NO 12062 WASHINGTON, DC
POSTAGE WILL BE PAID BY DEPARTMENT OF THE ARMY

Director
US Army Ballistic Research Laboratory
ATTN: DRSMC-BLA-S (A)
Aberdeen Proving Ground, MD 21005

FOLD HERE

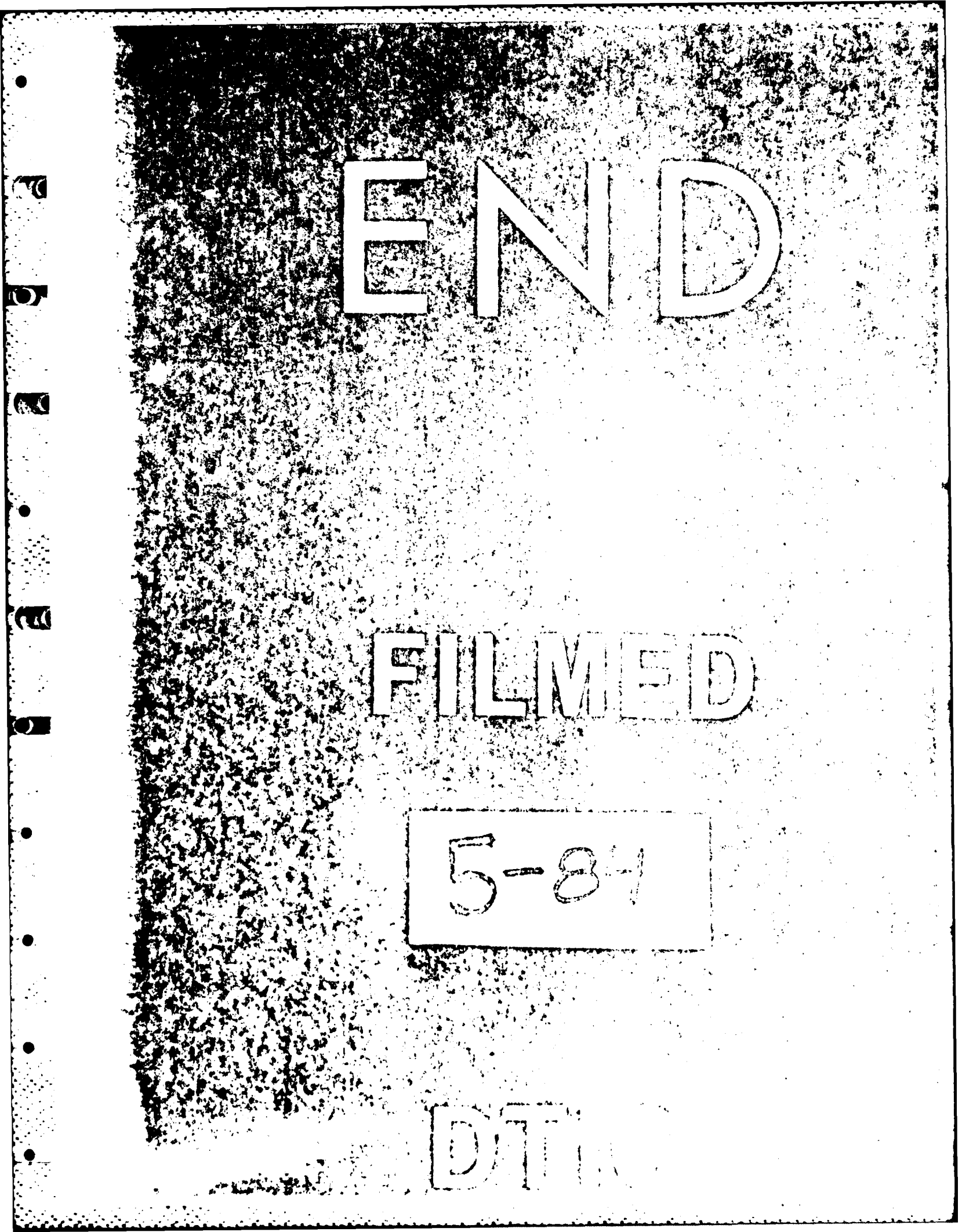
END
FILMED
5-84
DTIC